Fourth and Final Report
EAA Project 1.B: GCC-Specific DOAS with High Latent Effectiveness

Masdar Institute

Research Progress Report for Period ending 31 Mar 2015

Principal Investigator: Peter Armstrong

Principal Contributors: M. Tauha Ali, Omer Sarfraz

Project Start Date: 8 November 2012

Sponsor: Executive Affairs Authority of Abu Dhabi

EXECUTIVE SUMMARY

Different DOAS configurations are explored for satisfying the ventilation cooling demand efficiently in the Abu Dhabi climate. In the second quarter progress report, it was found that elimination of reheat from the DOAS system with only ERW and an air-cooled chiller satisfying sensible cooling demand results in 15% annual total cooling energy savings as compared to a conventional VAV system. Reheating coils for minimizing reheat energy have been proposed as early as (1966) by Rharnish. Different DOAS configurations for minimizing the reheating energy were explored which included using of 1) an air-subcooler in parallel with HW, 2) in series with HW, 3) water-subcooler utilizing condensed water and 4) using HW between supply and return air streams.

It was found that placing the run-around HX across evaporator is more efficient than placing the HX between supply and return air streams. However, condensation control is required to avoid condensation in the run-around HX. It was also found that the energy efficiency of placing a reheat coil in parallel with the HW is around 7% more efficient than placing the reheat coil in series to the HW after the evaporator. However, while reduced reheat energy results in 7% overall efficiency increase, the DX energy consumption of the latter case increases due to reduction in recovery rate across the run-around heat exchanger resulting from unbalanced flow.

An analysis of a closed DOAS system was made using different combinations of ERW and HW effectiveness. It was found that for high absolute humidity conditions of around 30 g/kg, the amount of water produced by the evaporator is close to the water amount required for condensation. Annual water use for an evaporatively cooled condenser is thus very small and the closed DOAS (attractive because it eliminates the outdoor unit) is shown to be feasible.

Lastly, LCC optimization is performed for finding optimum ERW and HW effectiveness and establishing a threshold for feasibility of using a separate DOAS system for latent load handling for GCC climates. It was found that the optimum ERW and HW effectiveness for conventional DOAS is around 0.86. For DOAS with air-subcooler, ERW effectiveness is optimum around 0.8-0.85 for climates having greater than 500 FLEOH while HW effectiveness is found to range between 0.74-0.82. Installation of a separate ventilation system for handling latent load was found to be feasible for all GCC climates with greater than 500 FLEOH

A high performance DOAS specification for GCC climate was developed in collaboration with DRI ROTOR, a major global OEM for AHU with energy recovery wheels.

Table of Contents

EXECUTIVE SUMMARY 2

1. LITERATURE REVIEW 4

DOAS Benefits and Comparison with conventional VAV systems: 4

DOAS Configurations discussed in Literature: 6

2. COMPONENT AND SYSTEM MODELING OF PROPOSED DOAS CONFIGURATIONS IN MATLAB 7

Proposed DOAS Configurations: 7

DOAS Component Modeling: 10

DOAS Component Model Linking with Vapor Compression Equipment/Outdoor Unit: 11

DOAS Implementation 12

Sensible Heat Wheel Condensation and Sub-cooling/Reheating Control Description: 14

Run-around HX/Sensible Heat Wheel (HW) Condensation Control: 14

Sub-cooling/Reheating Control: 15

Closed packaged DOAS 16

Introduction ..... **Error! Bookmark not defined.**

First Law Modeling of Closed DOAS 16

Analysis 18

Results for all Cases 23

Discussion 26

3. LIFE CYCLE COST OPTIMIZED DESIGN FOR PROPOSED DOAS CONFIGURATION FOR GCC WEATHER DATA 27

GCC Weather Data Description: 27

Ventilation Load Description: 28

LCC-Optimized DOAS Configurations Performance for Abu Dhabi Weather: 29

LCC-Optimized DOAS with Air Sub-cooler Cases and conventional ERW and HW case for GCC Weather Stations: 31

4. REAL-WORLD DEMONSTRATION OF BEST LCC-OPTIMIZED DOAS CONFIGURATION 32

5. CONCLUSIONS ..... **Error! Bookmark not defined.**

6. REFERENCES 36

Appendix A 40

1. Literature Review

For all-air systems, the room temperature, humidity and ventilation rates are all controlled through the supplied air, and are therefore strongly influenced by the supply conditions. In multi-zone buildings, in which the supply conditions are determined, based on a critical (aka most-needy) zone, it can be difficult to maintain both the desired temperature and humidity in individual, non-critical zones. Moreover, in most cases different zones have different ventilation needs, and the ratio between the return and fresh air is determined based on a zone with the highest needs. This causes other zones to have larger amounts of fresh air than needed, and increases the energy consumption.

A strategy of decoupling the sensible (temperature) control from the latent (humidity) and ventilation control was suggested for improved indoor air quality (IAQ) and energy savings(Coad 1999; S. A. Mumma 2001; Fischer and Bayer 2003). In a decoupled system, ventilation and humidity are controlled by a dedicated outdoor air system (DOAS), which can also deliver a certain amount of sensible heating/cooling. The remaining sensible loads are met by a parallel system.

DOAS Benefits and Comparison with conventional VAV systems:

Larrañaga et al. (2008) discussed the advantages of using a DOAS for humidity control over conventional packaged HVAC systems. The packaged HVAC systems doing dehumidification have four cost penalties; increase in first cost of equipment associated with auxiliaries and electrical service as the packaged system needs to handle dehumidification, reheat coil cost, annual operating cost for sensible cooling of air to dew point and also for reheating of air. A DOAS on the other hand has the advantages of meeting comfort criteria with lower energy use, improved and independent temperature and humidity control, downsizing of auxiliaries such as fans/pumps and reheat equipment, higher temperature set-points due to increased evaporation from the skin of building occupants and flexibility of turning off sensible cooling equipment while providing dehumidification during unoccupied hours.

A thorough analysis of design considerations, advantages and possible disadvantages for a DOAS can be found in numerous papers by Mumma. Based on different DOAS supply air temperatures, (S. A. Mumma and Shank 2001) analyzed the capital and operating cost for the parallel sensible cooling system (chiller and terminal coil equipment). In the proposed system, the outside air first passes through an enthalpy wheel (transfer of heat and moisture), gets cooled and dehumidified further to a dew-point temperature of approximately 7°C by a DX or chilled water coil, and is reheated to the supply dry-bulb temperature of 13°C using a sensible wheel. When delivering the same amount of outside air, DOAS is an attractive technology compared to a conventional all-air system, based on the annual performance results for Atlanta (S. A. Mumma and Shank 2001). (S. A. Mumma 2010a) pointed out the importance of building pressurization for indoor air quality and the problem of reduction in enthalpy wheel efficiency for unbalanced flows. His analysis showed that for an office building with a leakage rate of 5 m3/(hr-m2) at 50 Pa, and compliance with ASHRAE Standard 62.1 ventilation requirements, the ratio of the pressurization flow to the total ventilation flow rate should be around 0.7 to achieve adequate pressurization.

(S. Mumma 2002) analyzed DOAS in combination with metal ceiling radiant cooling panels (CRCP). The condensation on the ceiling is prevented by maintaining the water inlet temperatures above the room dew-point temperature. The cost analysis showed that this system can lower both the capital and operating cost compared to a conventional VAV system by taking capex cost savings for the chiller and ductwork, as well as fan energy opex savings. (Jeong, Mumma, and Bahnfleth 2003a) compared a conventional VAV system with an air-side economizer, to the proposed system. The proposed system had CRCP sized to meet sensible loads, and a parallel, constant air volume DOAS sized to meet full latent, and a part of sensible loads. For small cooling loads, both latent and sensible loads were met solely by DOAS. As the load increased, DOAS supply temperature dropped until reaching the lower limit of 11°C. If the zone set point temperature was still not met, the radiant cooling system was turned on, and the water supply temperature was controlled to meet the remaining sensible loads. Compared to the VAV system, savings were 42% for the annual energy consumption and 50% for the peak energy achieved through enthalpy recovery, higher zone air temperature, higher chiller evaporator temperature, and reduced fan energy. (Jeong and Mumma 2003) also analyzed the influence of a convective heat transfer coefficient on the radiant panel cooling capacity. Although mixed convection (natural and forced) significantly enhanced a panel cooling capacity, the impact was small for discharge air velocities less than 2 m/s. In subsequent work, (S. A. Mumma and Jeong 2005b) gave control recommendations for the parallel DOAS and CRCP system. While testing the proposed control strategy in the real building, with the DOAS supply air temperature of 17°C, average CRCP temperature 16°C, room dry-bulb temperature 23°C and room dew-point temperature 12°C, the thermal comfort analysis showed very low Predicted Percent Dissatisfied (PPD) of 5% (S. A. Mumma and Jeong 2005a).

Emmerich and McDowell (2005) performed a simulation study of a two-story office building over five US climates, with and without DOAS. The analysis was done by combining TRNSYS for the building response and CONTAM for the infiltration and inter-zonal airflow. Compared to the base case, adding DOAS resulted in 14–37% annual energy cost savings. However, although DOAS had cooling coils intended to fully meet latent loads, a certain amount of latent cooling was still occurring on the parallel system because they used the same chilled water for both systems and the DOAS was sized only for maximum ventilation airflow rate. Similar cost savings for the combined radiant-DOAS system were shown in the field demonstration for the school in Florida (Khattar et al. 2003). In addition to an ice-storage system, the system had separate conditioning for the recirculation and ventilation air, with the ventilation air being cooled to lower temperatures (6°C) for dehumidification purposes. Compared to the school of a similar size and use, and with a conventional VAV system, the cost savings were 22%, with only 1% increase in the capital cost. It is also reported that the school with DOAS had much better humidity control.

There have been quite a few studies by Stetiu (1999); Mumma and Shank (2001); Jeong et al. (2003a) and Tian and Love (2009) comparing VAV systems with radiant-DOAS system. Stetiu (1999) compared a combined radiant-DOAS system to a VAV system with an air-side economizer. The analysis for a typical office was performed for a summer week, across 9 US climates, and for different latent fractions of the total cooling energy. The results showed that in all climates, even in a humid climate like New Orleans, the radiant cooling system with the supply water temperature of 20°C was able to maintain the indoor

temperature within comfortable 24°C, and without condensation problems. It was shown that the combined cooling system uses less energy compared to the all-air system for all climates, even with the continuous ventilation. The energy and the peak power savings were 17 – 42%, with lower savings corresponding to cold, moist climates with better potential for an air-side economizer. Jeong et al. (2003b) compared a conventional VAV system with an air-side economizer to ceiling radiant cooling panels with a parallel DOAS. The panels were sized to meet sensible loads and the parallel, constant air volume, DOAS was sized to meet full latent and a part of sensible loads. For small cooling loads, both latent and sensible loads were met solely by DOAS. Compared to the VAV system, savings were 42% for the annual energy consumption and 50% for the peak energy achieved through enthalpy recovery, higher zone air temperature, higher chiller evaporator temperature, and reduced fan energy. Niu et al. (1995) and Tian and Love (2009) included a water size economizer to the radiant-DOAS system. Similar to (Stetiu 1999), Tian and Love (2009) compared the continuous DOAS operation and the operation with over-night shutdown. The radiant-DOAS system performed better across 16 analyzed US climates, with annual cooling energy savings up to 60% for the night-time shutdown, and 40% for a continuous operation. The largest savings were reported for dry climates (hot and cold), while humid climates had lower savings due to the need for continuous ventilation for dehumidification purposes and fewer water-side relative to air-side economizer hours (less wet bulb depression). Armstrong et al. (2009) found that higher chilled water temperatures and shifting load to times of lower ambient temperatures resulted in savings of 20% to over 50% for sensible cooling. Savings of this magnitude were confirmed experimentally by (Gayeski, Armstrong, and Norford 2012).

For a typical office building in Denver, Colorado, (Moore 2008) analyzed a hydronic radiant system in slabs, combined with DOAS and a cooling tower. The system saved around 60% energy over the whole cooling season, compared to a conventional VAV system with an air-side economizer. In addition to fan energy savings, significant chiller savings result from the fact that in a dry climate, wate-side economizer temperatures are much lower than air-side economizer temperatures. The reported Predicted Percentage of Dissatisfied (PPD) was below 10%.

DOAS Configurations discussed in Literature:

Gatley (2000) gave a detailed overview of different dehumidification options and suggested several energy efficient alternatives to conventional reheat coils, such as coil-loop run-around, heat-pipe runaround, air-to-air heat exchanger, rotary-wheel heat exchanger, and the arrangement in which, after passing through the condenser, the refrigerant passes through an additional coil used to transfer heat from the refrigerant to the air. In this way the refrigerant is sub-cooled, resulting in an increased enthalpy difference on the evaporator. Wallin et al. (2012) showed a 47% annual savings by heat recovery using a run-around coil in the DOAS.

Energy recovery based DOAS cooling systems aim to minimize cooling and reheating loads by changing the evaporator inlet conditions. Zhang et al. (2005) and Zhang (2006) presented different DOAS configurations to reduce the cooling load and minimize reheat energy to achieve desired supply air conditions. The DOAS configuration in which hot refrigerant from the condenser was used for reheating

resulted in a maximum savings of 42% compared to DOAS with simple DX dehumidification without energy recovery. The reheating of dehumidified air using condensers in the supply air streams have been proposed by Rharnish (1966). These reheat coils can be designed to provide subcooling of refrigerant which enhances the vapor compression equipment performance (Katipamula 1997). Patents by Eber et al. (2002) and Trent (2003) proposed DOAS which consisted of reheat coils with subcooling performed primarily in the outdoor air or the supply air respectively.

2. Component and System Modeling of DOAS

Five different DOAS configurations were developed to reduce the dehumidification and reheating load based on the efficiency enhancing techniques found in the literature. First principle models of the components were developed using OEM literature and data present in the published literature. Annual simulation of the five configurations were performed by linking the DOAS component models with vapor compression equipment.

Candidate DOAS Configurations:

(a)

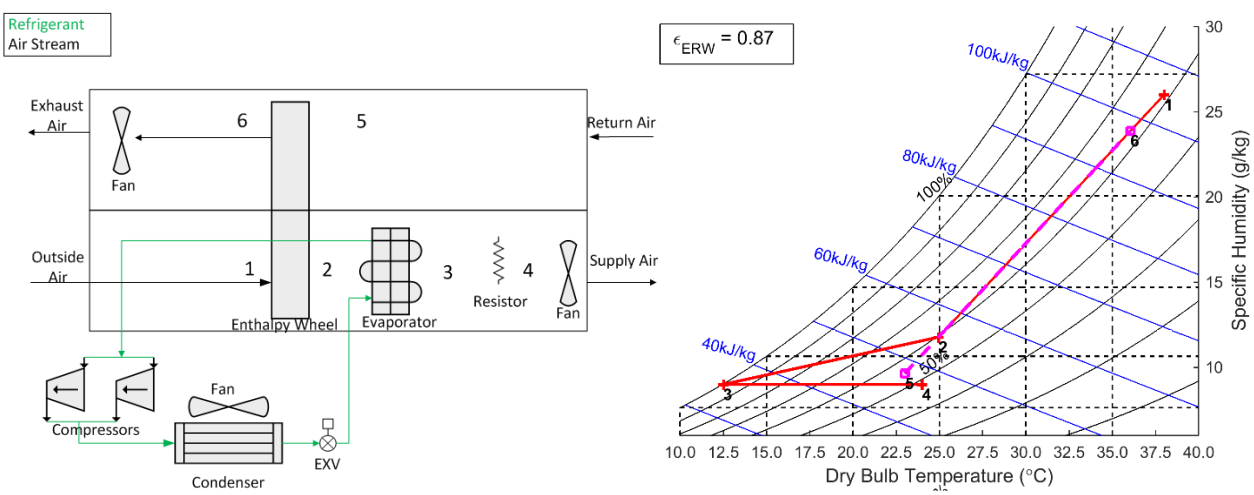

(b)

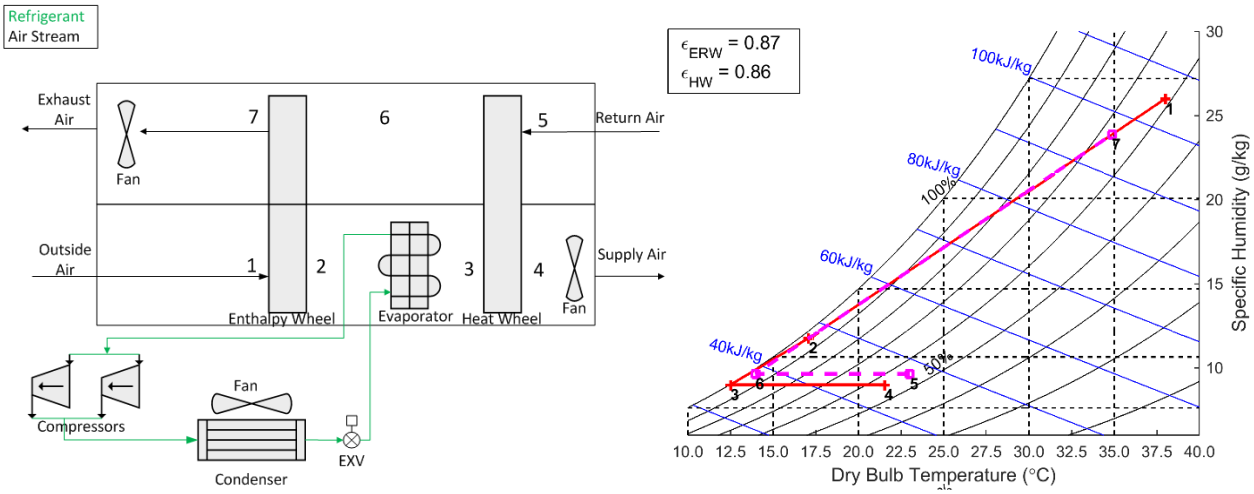
Refrigerant
Air Stream
Exhaust Air
Fan
Return Air
Outside Air
Supply Air
Enthalpy Wheel
Evaporator
Heat Wheel
Compressors
Condenser
EXV
ϵ_{ERW} = 0.87
ϵ_{HW} = 0.86
100kJ/kg
80kJ/kg
60kJ/kg
40kJ/kg
100%
50%
Specific Humidity (g/kg)
Dry Bulb Temperature (°C)

(c)

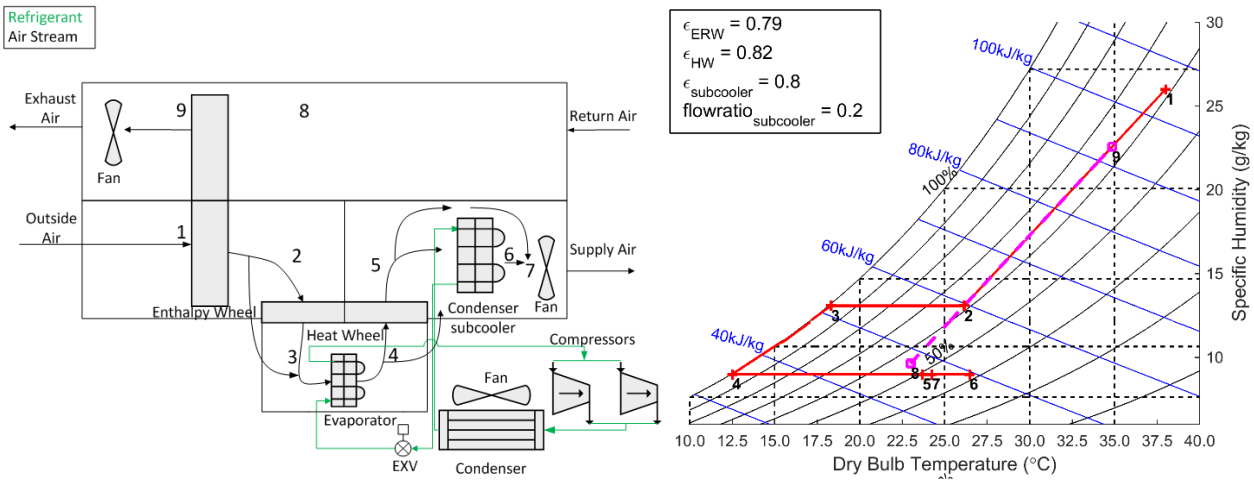
Refrigerant
Air Stream
Exhaust Air
Fan
Return Air
Outside Air
Supply Air
Enthalpy Wheel
Heat Wheel
Condenser subcooler
Compressors
Evaporator
EXV
Condenser
ϵ_{ERW} = 0.79
ϵ_{HW} = 0.82
$\epsilon_{subcooler}$ = 0.8
flowratio$_{subcooler}$ = 0.2
100kJ/kg
80kJ/kg
60kJ/kg
40kJ/kg
100%
50%
Specific Humidity (g/kg)
Dry Bulb Temperature (°C)

(d)

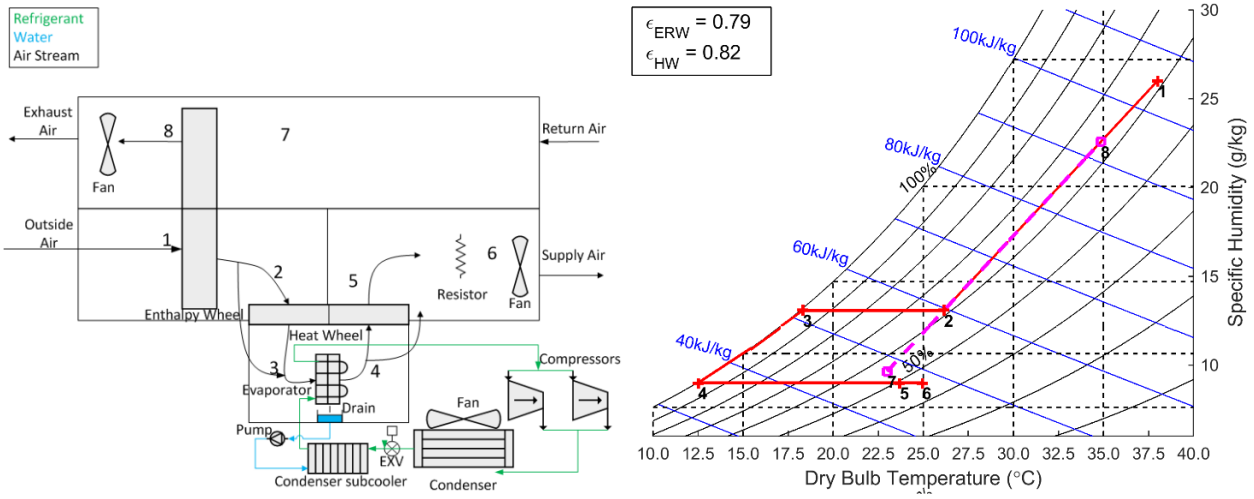
Refrigerant
Water
Air Stream
Exhaust Air
Fan
Return Air
Outside Air
Supply Air
Resistor
Enthalpy Wheel
Heat Wheel
Compressors
Evaporator
Drain
Pump
EXV
Condenser subcooler
Condenser
ϵ_{ERW} = 0.79
ϵ_{HW} = 0.82
100kJ/kg
80kJ/kg
60kJ/kg
40kJ/kg
100%
50%
Specific Humidity (g/kg)
Dry Bulb Temperature (°C)

(e)

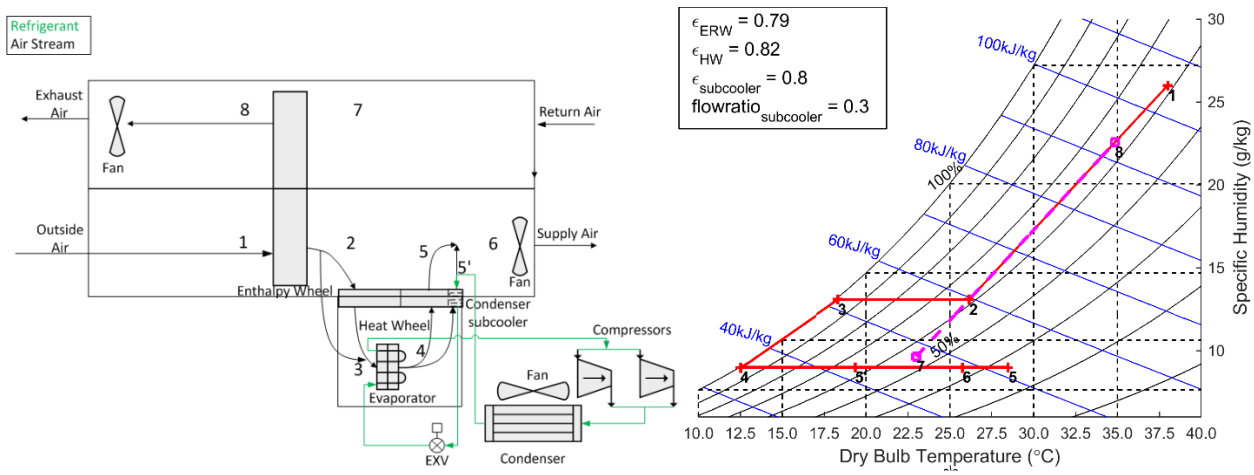

Figure 1: (a) Base case DOAS with ERW (b) DOAS with ERW and HW between SA and RA (c) DOAS with ERW, a run-around HW and air-subcooling/reheating coil in series to HW (d) DOAS with ERW, a run-around HW and water-subcooling HX (e) DOAS with ERW, an un-balanced run-around HW and air-subcooling/reheating coil in parallel to HW

Figure 1 presents the proposed DOAS configurations schematic along with the Outdoor air (OA) and return air (RA) states on the psychrometric chart. Case (a) represents the commonly used DOAS configuration with Enthalpy Recovery Wheel (ERW) while case (b) represents the conventional high efficiency DOAS configuration with ERW and Heat Wheel (HW) sold by DOAS manufacturers. Cases (c)-(e) explores the use of a run-around HW for simultaneous cooling coil's thermal load reduction and reheating of cold air along with including an additional Heat Exchanger (HX) for subcooling the refrigerant for enhancing DX cycle efficiency. Life cycle cost (LCC) optimized effectiveness (ε) of ERW and HW for an air-cooled condenser DX-DOAS with balanced air flow in the Supply Air (SA) and RA streams are given on the psychrometric charts at the outdoor Abu Dhabi design conditions of 38°C dry bulb temperature (*T*) and 26g/kg specific humidity (*w*) occurring at maximum wet bulb temperature of 31°C based on ASHRAE's IWEC TMY[1] data. The off-coil condition is considered as *T*=12.5°C and *w*=9g/kg which corresponds to the specific humidity at zone conditions of *T*=24°C and 50% relative humidity (RH). The return air state is considered as T=23°C and *w*=9.65g/kg based on AHRI Standard 1061 (2013). Equations (1-9) are used to estimate the air states across the heat exchangers. The saturated condenser liquid refrigerant approach temperature for cases (c) and (e) is taken as 3K. For case (e), subcooler (SC) outlet temperature calculations are done using $\dot{m}_{sc}$ given by Eq. (8) in place of $\dot{m}_{SA}$. The refrigerant fluid properties are taken at the inlet condition of the heat exchangers while the air properties are assumed constant i.e. $\rho_{air} = 1.2\ kg/m3; C_{p_{air}} = 1006\ J/kg$

For cases (a)-(e):

[1] ASHRAE's IWEC TMY: American Society for Heating Refrigeration and Air-conditioning Engineering's International Weather for Energy Calculations Typical Meteorological Year

$$\varepsilon_{ERW} = \frac{\dot{m}_{SA}}{\dot{m}_{RA}} * \frac{T_{OA} - T_{SA}}{T_{OA} - T_{RA}};\ \varepsilon_{ERW} = \frac{\dot{m}_{SA}}{\dot{m}_{RA}} * \frac{w_{OA} - w_{SA}}{w_{OA} - w_{RA}} \quad (1)$$

$$Q_{ERW} = \dot{m}_{SA} * C_{p_{air}} * (T_{OA} - T_{SA}) = \dot{m}_{RA} * C_{p_{air}} * (T_{ERWexhaust} - T_{RA}) \quad (2)$$

For case (b):

$$\varepsilon_{HW} = \frac{\dot{m}_{SA}}{\dot{m}_{RA}} * \frac{T_{SA} - T_{EvapSA}}{T_{RA} - T_{EvapSA}} \quad (3)$$

$$Q_{HW} = \dot{m}_{SA} * C_{p_{air}} * \left(T_{SA} - T_{EvaporatorSA}\right) = \dot{m}_{RA} * C_{p_{air}} * (T_{HWRA} - T_{RA}) \quad (4)$$

For case (c)-(e):

$$\varepsilon_{HW} = \frac{\dot{m}_{HWin}}{\dot{m}_{HWout}} * \frac{T_{ERWSA} - T_{Evapinlet}}{T_{ERWSA} - T_{EvapSA}};\ \varepsilon_{sc} = \frac{\dot{m}_{SA} * C_{p_{air}}}{(\dot{m} * C_p)_{min}} * \frac{T_{SA} - T_{HWSA}}{T_{satcondliq} - T_{HWSA}} \quad (5)$$

$$Q_{HW} = \dot{m}_{HWin} * C_{p_{air}} * \left(T_{ERWSA} - T_{Evapinlet}\right) = \dot{m}_{HWout} * C_{p_{air}} * \left(T_{HWSA} - T_{EvaporatorSA}\right) \quad (6)$$

$$\frac{\dot{m}_{SA} * C_{p_{air}}}{(\dot{m} * C_p)_{min}} = \frac{\dot{m}_{SA} * C_{p_{air}}}{\dot{m}_{SA} * C_{p_{air}} * (T_{Evaporatorinlet} - T_{EvaporatorSA})/h_{fg_{refrigerant}} * C_{p_{refrigerant}}} \quad (7)$$

For case (e):

$$\dot{m}_{sc} = \dot{m}_{HWin} - \dot{m}_{HWout}; \dot{m}_{HWin} = \dot{m}_{SA} \quad (8)$$

$$T_{SA} = \frac{\dot{m}_{sc} * T_{scSA} + \dot{m}_{HWout} * T_{HWSA}}{m_{SA}} \quad (9)$$

DOAS Component Modeling:

The outdoor unit model is based on the heat pump model of (T. Zakula et al. 2011). The outdoor unit model is optimized for compressor speed and condenser air flow rate over a range of capacity fraction (*CF*), condenser inlet air temperatures (*Tx*) and evaporating temperatures (*Te*). Polynomial fits as function of *CF*, *Tx* and *Te* are fitted to the *1/COP* and $T_{satcondliq}$ model presented in Figure 2. The fixed parts of the compressor and condenser fan inverter loss model presented in (T. Zakula et al. 2011) are removed to achieve curve-fits with low root mean squared error 'RMSE' with lower order polynomials. The details of the polynomial fits is presented in Appendix A.

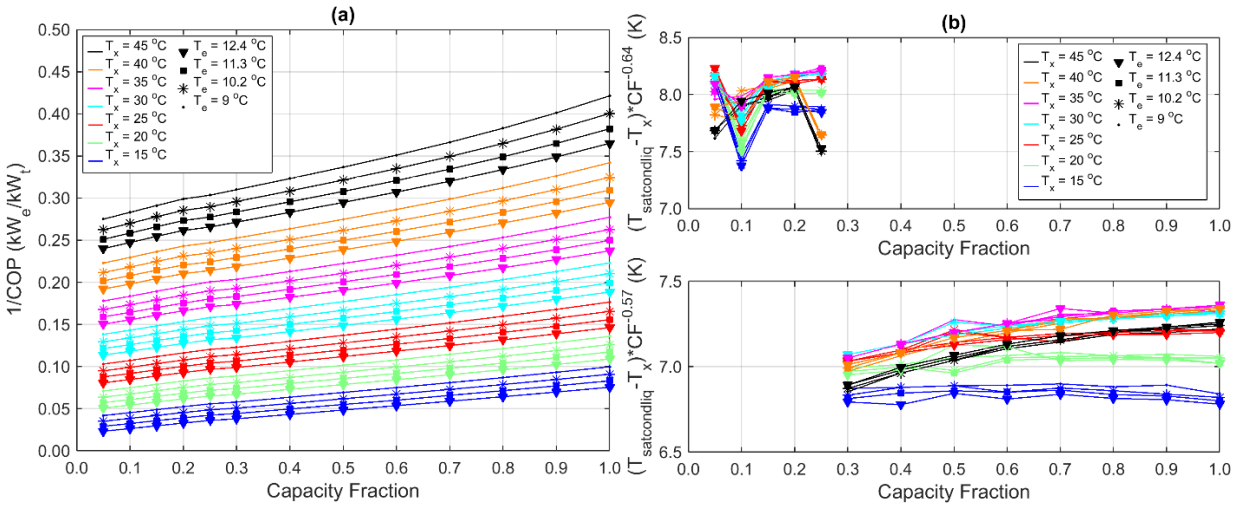

Figure 2: (a) Air cooled outdoor unit 1/COP vs. CF map for different Tx and Te (b) Air cooled outdoor unit Tcondliq model vs. CF for different Tx and Te

Coupling of DOAS Model with Vapor Compressor/Condenser Unit:

The performance of outdoor unit i.e. compressor, condenser, oil heat exchangers, suction subcoolers etc. depends mainly on the capacity fraction, condenser inlet air conditions and the refrigerant-side suction conditions. This concept is used to generate compressor performance data in compressor calorimeters (Stoecker and Jones 1982; Duggan et al. 1988; ASHRAE 23.1-2005; Willingham 2009). The methodology presented here extends this approach for modeling of systems with complex load-side conditions such as DOAS.

The cooling system model is divided into two parts: Outdoor unit and Indoor unit. Outdoor unit deals with the vapor compression cycle components except load-side heat exchangers (evaporators) and valves while the Indoor unit deals with the remaining components of the cooling equipment such as evaporator, expansion valve and optional components such as enthalpy recovery wheel, heat wheel and refrigerant subcoolers.

The outdoor unit consists mainly of compressor and condenser heat exchanger. Efficiency improving components such as compressor economizer, suction side subcooler, compressor and condenser fan motor inverters, compressor motor oil cooler, oil separator etc. can be added to the outdoor unit model. The compressor is modeled using semi-empirical modeling approach described in (T. Zakula et al. 2011; Javed et al. 2014; Cheung and Braun 2014). Outdoor unit heat exchangers are modeled based on the effectiveness, ε-NTU approach with moving boundary method (Hiller and Glicksman 1976; Browne and Bansal 2001; T. Zakula et al. 2011) to account for vapor-side pressure drop and variations in number of transfer units (NTU) with refrigerant mass flow rate, *mref*. The outdoor unit component models along with a heat balance model of evaporator described by Eq. (11) is solved with an initial guess of condensing pressure, *Pcond*, and condenser refrigerant liquid enthalpy, *hcondliq*, for the operating

range of capacity fraction (CF), evaporating temperature, *Te*, and condenser entering air temperature, *Tx*. The initial guess of *Pcond* and *hcondliq* are estimated at saturated liquid conditions for a condenser approach of 3K.

$$CF = \frac{\dot{Q}_{cooling}}{\dot{Q}_{rated}} \quad (10)$$

$$Q_{cooling} = \dot{m}_{ref} * \left(hevap_{in} - h_{evapout}\right) + \dot{m}_{ref} * cp_{ref} * \left(T_{superheat} - Te\right) \quad (11)$$

Polynomial curve fits for specific power (1/COP) without fixed part of inverter losses for compressor and condenser fan and condenser's saturated leaving liquid temperature, *Tcondliq*, are generated as a function of CF*, Te and Tx.* The load-side heat and mass exchanger of the cooling system are modeled based on the ε-NTU approach to determine *Te* using interval bisection for satisfying the given cooling load. The cooling load is estimated by Eq. (12).

$$\dot{Q}_{cooling} = \dot{m}_{evapair} * \left(h_{evapair_{in@T_{evapair_{in}},w_{evapair_{in}}}} - h_{evapair_{out@LDPT}}\right) \quad (12)$$

The electrical power of the equipment is calculated from the 1/COP curve fit for the given CF*, Te* and *Tx.*

DOAS Implementation

DOAS with energy recovery devices present a load-side case where the cooling system power is dependent on the psychrometric state of air entering the cooling coil, the air ventilation flow rate required to satisfy fresh air demand, desired supply air state and the effectiveness of heat exchangers used to reduce reheating and/or enhance the cooling effect by refrigerant subcooling. This large a number of load-side boundary conditions preclude the use of empirical system curve fits for estimating cooling system performance with accuracy or for performing optimization of system parameters and/or controls.

The modeling approach described above enables the modeling of load-side conditions based on first principles approach as effectively only one variable *Te* needs to be solved for predicting cooling system performance from empirical curve fits of outdoor unit model. **Error! Reference source not found.** shows the schematic of a balanced DOAS with a run-around heat wheel and refrigerant subcooler doing reheating of cold air and subcooling of refrigerant.

The algorithm for estimating *Te* for a given cooling load for vapor compression equipment with subcooler shown in **Error! Reference source not found.** is described below:

1. Polynomial fits as a function of CF*, Tx/Tx* and *Te* for 1/COP and *Tcondliq* are performed for the data obtained from outdoor unit's simulation over the operating range

2. Interval bisection method is used to estimate the *Te* for a given cooling load by minimizing the sum of errors in estimating capacity fraction, condenser liquid temperature and evaporator energy balance

a. The Load side model is solved for the initial conditions defined as the desired leaving dew point temperature '*LDPT*' and three degrees below *LDPT*. This establishes the upper and lower error bounds with opposing signs

   i. If the error at lower limit doesn't result in opposing signs then the *Te* lower limit is decreased until errors with opposing signs are obtained for the higher and lower *Te* limits

b. The load-side model is solved at given *Te* using the following steps:

   i. Enthalpy recovery wheel 'ERW' effectiveness is calculated based on (Simonson and Besant 1999) to determine the moist-air state entering the sensible heat wheel. The inputs to the model are the outdoor air (OA*)* and return air (RA) flow rates, temperatures '*T*' and specific humidities '*w*'. The effectiveness 'ε' equations for the ERW are described by Eq. (13) & (14):

$$\varepsilon_{ERW} = \frac{\dot{m}_{evapair,SA}}{\dot{m}_{evapair,RA}} * \frac{T_{air,OA} - T_{air,HW_{ERWin}}}{T_{air,OA} - T_{air,RA}} \qquad (13)$$

$$\varepsilon_{ERW} = \frac{\dot{m}_{evapair,SA}}{\dot{m}_{evapair,RA}} * \frac{w_{air,OA} - w_{air,HW_{ERWin}}}{w_{air,OA} - w_{air,RA}} \qquad (14)$$

   ii. Sensible heat wheel model 'HW' effectiveness is computed based on (Wu, Melnik, and Borup 2006) to compute the air inlet temperature entering the evaporator using Eq. (13). The inputs to the model are leaving air temperatures and flow rates of *ERW* and evaporator.

   iii. The CF of the vapor compression equipment is estimated from the desired *LDPT* and air flow rate using Eq. (10) & (11)

   iv. If the CF is lower than the optimal CF estimated from the 1/COP map for given *Tx* and *Te*, the air flow rate is changed and iteration is done by solving enthalpy wheel and sensible wheel models to compute the amount of air flow required and evaporator inlet enthalpy condition to obtain optimal CF

   v. *Tcondliq* is computed using the cubic polynomial obtained from curve fit of outdoor unit data as a function of CF, *Tx* and *Te*

   vi. The refrigerant-air subcooler model is based on the counterflow ε-NTU heat exchanger model. The inputs to the model are *Tairsc, Tcondliq, mref* and *mevapair+mpressair*. The expansion valve (EXV) entering enthalpy '$hEXV_{in}$' is obtained from $TEXV_{in}$ and *Pcondliq* calculated at *Tcondliq* using Eq. (15):

$$T_{airsc} = \frac{T_{evapair,HWout} * \dot{m}_{evapair} + LDPT * \dot{m}_{pressair}}{\dot{m}_{evapair} + \dot{m}_{pressair}} \qquad (15)$$

vii. The evaporator model is solved using the wet cooling coil approach described in (Threlkeld 1970; Braun et al. 1989) to satisfy the evaporator energy balance given by Eq. (16). The inputs to the model are *Qcooling, hEXV*$_{in}$*, Te, mair, Tevapair*$_{in}$ and *wevapair*$_{in}$

$$\dot{Q}_{cooling} = \dot{Q}_{evap,dry} + \dot{Q}_{evap,wet} \quad (16)$$

viii. CF is corrected by subtracting the subcooling heat from the cooling load and CF error between the corrected CF and actual CF is computed

ix. The *Tcondliq* error is computed by subtracting the new *Tcondliq* based on the estimate of the corrected CF from the *Tcondliq* computed at actual CF

c. *Te* is said to be converged if the error sum is less than 0.1 or if *Te* step resolution has become less than 0.01K

3. The cooling equipment power is then computed by the *1/COP* performance map using *Tx* and the solved CF and *Te* parameters. The fixed parts of the inverter losses for the compressor and condenser fan are added back to obtain actual power consumed

   a. If the CF at the desired air flow rate was less than the optimal CF then the system power is multiplied by the operating fraction calculated by Eq. (17)

$$operating\ fraction = \frac{Q_{cooling}}{Q_{rated} * CF_{optimal}} \quad (17)$$

The refrigerant properties for the load-side are calculated based on saturated conditions at *Te* and *Tcondliq* using cubic polynomial fits of Refprop (Lemmon et al. 2007) saturated temperatures data for the range of -5°C to 50°C. The estimates of the cubic polynomial fits are provided in Appendix A.

Sensible Heat Wheel Condensation and Sub-cooling/Reheating Control:

Run-around HX/Sensible Heat Wheel (HW) Condensation Control:

The air flow through the HW (run-around heat exchanger) is controlled to avoid condensation which would lead to an increase in humidity ratio after dehumidification has been done by the evaporator. The air flow entering the heat wheel after the evaporator is bypassed to maintain the relative humidity of the air entering the evaporator below saturation. If the air entering the heat wheel at the hot side i.e. after the ERW is saturated then the HW is bypassed. The air flow passing through the HW to total air flow ratio is changed in steps of 10% to avoid condensation.

Sub-cooling/Reheating Control:

The sub-cooling/reheating control is implemented to avoid excessive reheat of air after the SC or HW. A desired zone supply temperature is chosen and the air flow through the HW or SC to total air flow ratios are changed in steps of 10% to maintain the desired temperature within 2K.

The control strategy for the DOAS configuration in which the air SC is placed in series of HW is implemented as follows:

1. If the air coming out of the HW is above the desired supply temperature then the air flow ratio at the hot side of heat wheel is decreased
2. The air SC is operated only if the air entering the sub-cooler is less than entering saturated liquid refrigerant temperature and the desired supply temperature
3. If the air coming out of the SC is greater than the desired supply temperature then the air flow ratio through the SC is decreased

The control strategy for the DOAS configuration in which the air SC is placed in parallel of HW is implemented as follows:

1. An initial air flow ratio of 10% is chosen to check whether condensation is occurring in the HW
2. The air SC is operated in balanced thermal capacitance mode if condensation has not occurred in the HW
3. If condensation has occurred in the HW then air flow ratio through the cold side of the HW determined by the condensation control takes precedence
4. If the supply temperature is greater than the desired setpoint or their difference is more than 2K:
    a. If the air temperature leaving the HW is greater than the setpoint temperature then the air flow ratio at the hot side of the HW is reduced
    b. If the air temperature leaving the subcooler is greater than the setpoint temperature then the airflow ratio at the cold side of HW is increased if the increase remains less than 1
    c. If the air temperature leaving the subcooler is less than the setpoint temperature then the airflow ratio at the cold side of HW is decreased and the air flow ratio at the hot side of HW is increased if it is less than 1

Closed Packaged DOAS

Water is obtained as a result of dehumidification of outdoor air in the evaporator. The amount of condensed water obtained depends on the specific humidity of the air. This water can be utilized to increase the performance of the heat pump. Condenser water from the evaporator can be used to remove the heat from the refrigerant in the condenser. For humid climates, one may surmise that the amount of condensed water could be sufficient to remove the heat of condensation of the refrigerant. The schematic of a closed DOAS is shown in Figure 3. The condensed water is sprayed on to the air entering the condenser to bring it near its saturation point. Some part of the condensed water is sprayed directly on to the coils of the condenser to increase the heat transfer coefficient that will result in better heat transfer. . The air after the condenser is still cool to perform desuperheating of the refrigerant. Not only this, the condensed water is also passed through a sub-cooler which improves the performance of the heat pump further by lowering the liquid refrigerant temperature. The lower condensing temperatures results in lowering pressure ratio which in turn decreases compressor work and increases COP.

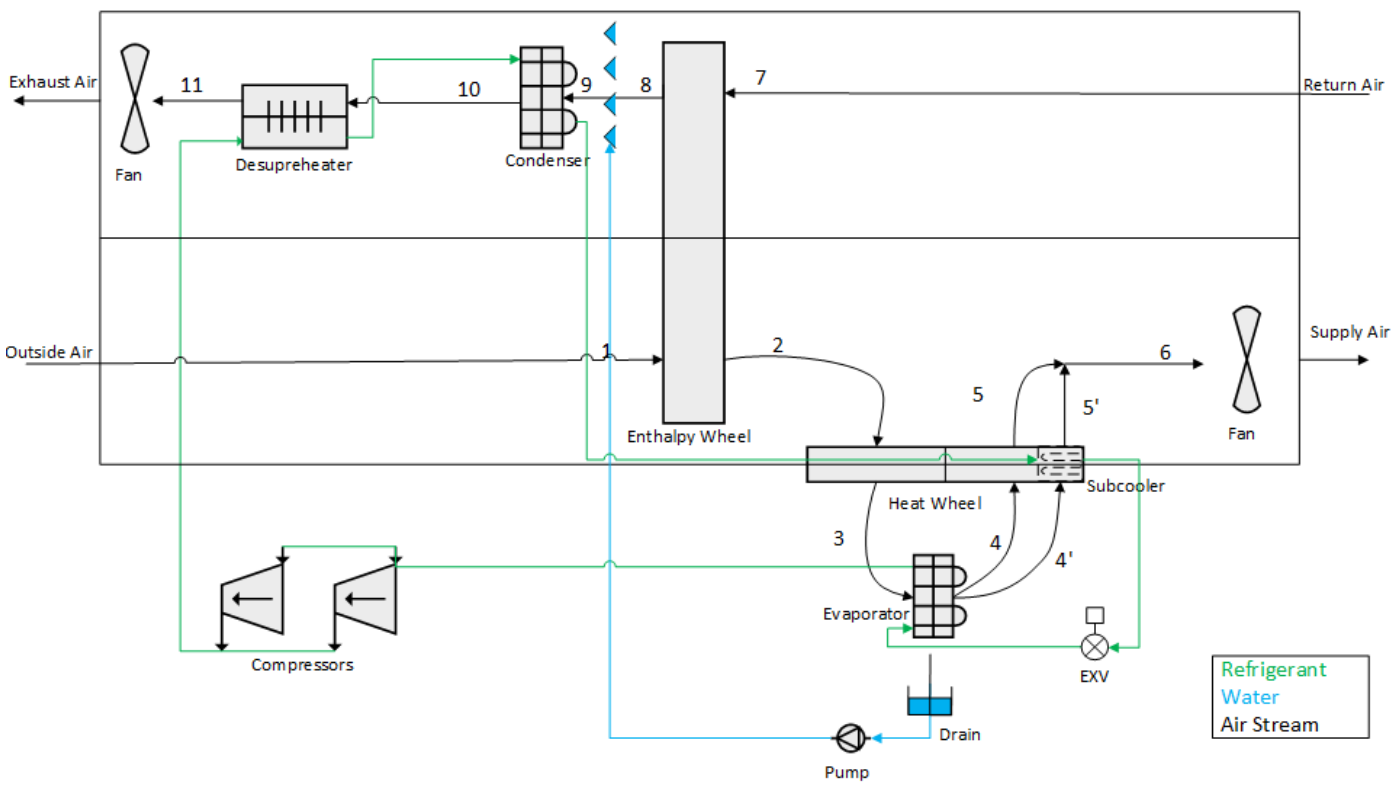

Figure 3: Schematic of closed DOAS

First Law Modeling of Closed DOAS

The feasibility analysis is carried out by assuming different values of effectiveness for heat wheel and enthalpy wheel. Outdoor air to be conditioned is passed through the enthalpy wheel where it exchanges heat and moisture with the return air stream. After the enthalpy wheel, air is passed though the heat

wheel to be sensibly cooled to near saturation condition. The nearly saturated air is then latently cooled by the evaporator such that air leaving the evaporator is at a cooler and dryer point on the saturated line (4) shown in Figure 4. The air leaving the evaporator is controlled to a specific humidity of 9g/kg which corresponds to 24°C dry bulb temperature and 50% relative humidity. For feasibility analysis, the evaporation surface temperature is therefore assumed to have a constant value of 12°C. Using $\dot{Q}_{evap}$,the mass flow rate of refrigerant is calculated as follows:

$$\dot{Q}_{evap} = \dot{m}_{ref} h_{fg\,ref,e} \quad (18)$$

For evaporator, water obtained by the condensation of moisture is obtained as:

$$\dot{m}_{w,evap} = \dot{m}_a \left(w_{evap,in} - w_{evap,out}\right) \quad (19)$$

where air leaving the evaporator is assumed to have a constant specific humidity of 9 g/kg.

After passing through the enthalpy wheel (7-8), the return air is adiabatically cooled (8-9) by part of water obtained from evaporator and rest of water is utilized to complete the condensation process. Checking whether water obtained from the evaporator is sufficient for adiabatic cooling of air and refrigerant condensation proceed as follows:

The air after adiabatic cooling is assumed to be fully saturated with wet bulb temperature same before and after this process. i.e.

$$T_{wb,Ew,out} = T_{wb,adiab,c} \quad (20)$$

Using these two conditions, dry bulb temperature, absolute humidity and enthalpy of air are calculated. The water required for adiabatic cooling is calculated using following relation:

$$\dot{m}_{w,adiab} = \dot{m}_a \left(w_{adiab,c1} - w_{EW,out}\right) \quad (21)$$

The $\dot{Q}_{cond}$ (for refrigerant, R410a) is given as follow:

$$\dot{Q}_{cond} = \dot{m}_R h_{fg,c} = \dot{m}_a (h_{c2} - h_{adiab}) \quad (22)$$

Air dry bulb temperature after condensation , $T_{a,cout}$, is obtained by solving the above equations.

The refrigerant condensing temperature is calculated from the air temperature at the condenser outlet using an assumed approach temperature of 3K, i.e.

$$T_{R,c} = T_{a,cout} + 3 \quad (23)$$

Using$\dot{Q}_{cond}$, the required mass of water is calculated as:

$$\dot{Q}_c = \dot{m}_{w,c} h_{fg,w} \quad (24)$$

Total water mass flow required $\dot{m}_{total}$ is calculated as:

$$\dot{m}_{total} = \dot{m}_{\ w,adiab} + \dot{m}_{w,c} \quad (25)$$

Analysis

Application of the above procedure is shown in the figures below.

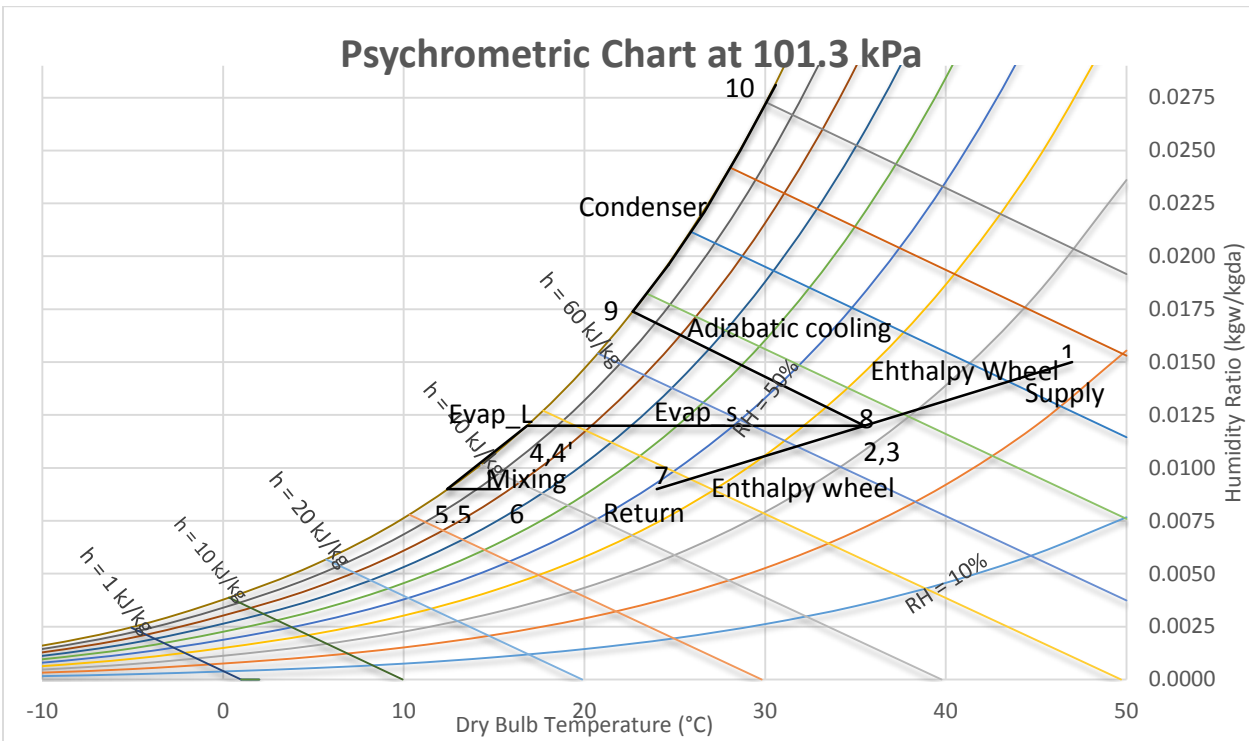

Figure 4: First case: EW sensible effectiveness = 0.5, EW latent effectiveness = 0.5, HW effectiveness = 0.0, outdoor air at 47 °C, 15 g/kg

In the case illustrated in Figure 4, air leaving the heat wheel is far from saturation. Therefore, in the evaporator, air is first sensibly cooled and brought to its saturation point and after that it is cooled on the saturation line mainly by moisture removal (latent cooling).

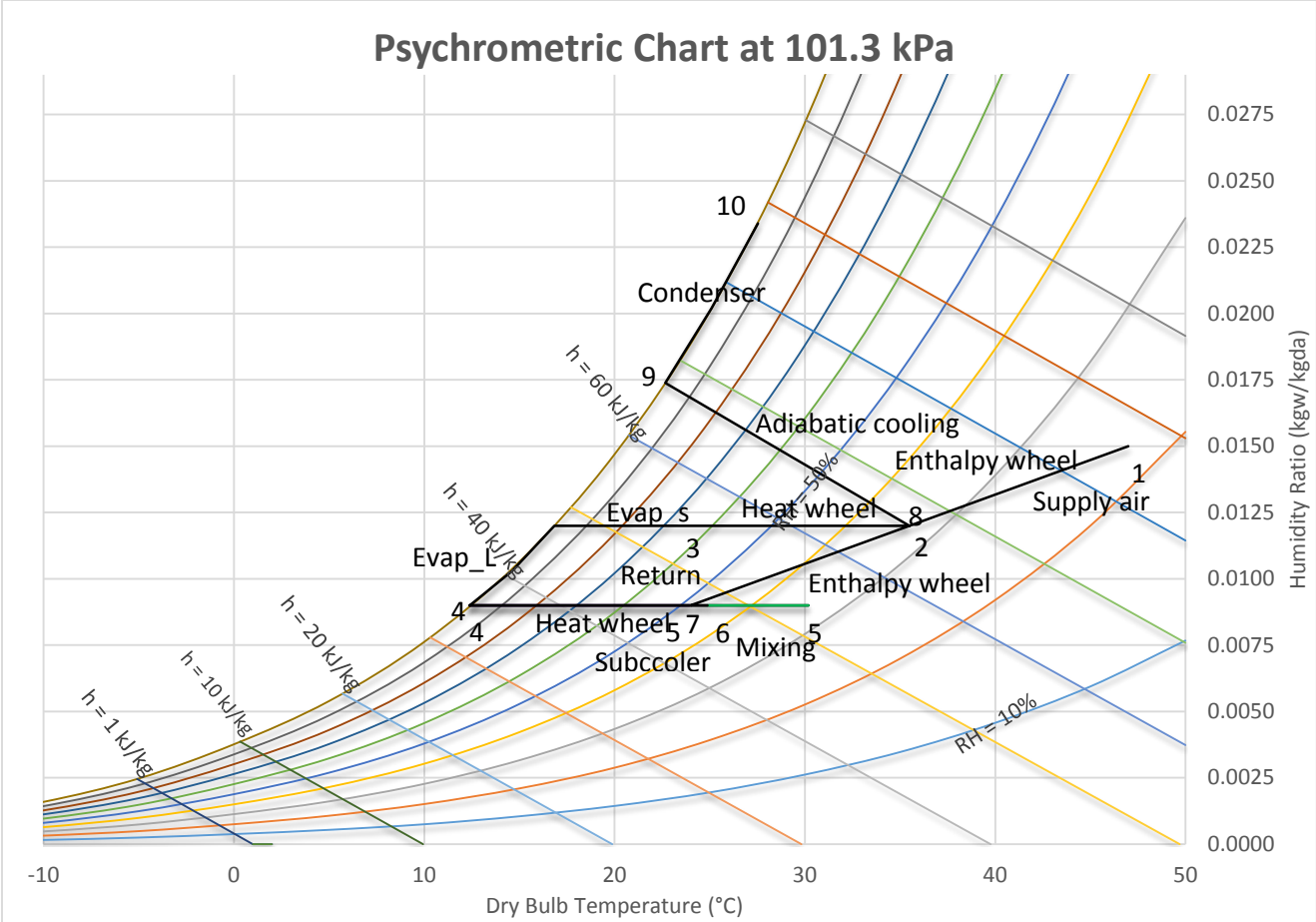

Figure 5: Second case: EW sensible effectiveness = 0.5, EW latent effectiveness = 0.5, HW effectiveness = 0.5, outdoor air at 47 oC, 15 g/kg

In second case shown in Figure 5, heat wheel effectiveness is increased to 0.5 while keeping the enthalpy wheel sensible and latent effectiveness constant. It can be observed from the above figure that as a result of precooling in the heat wheel, the part of sensible load is reduced. Therefore, evaporator will handle the remaining sensible load and the latent load.

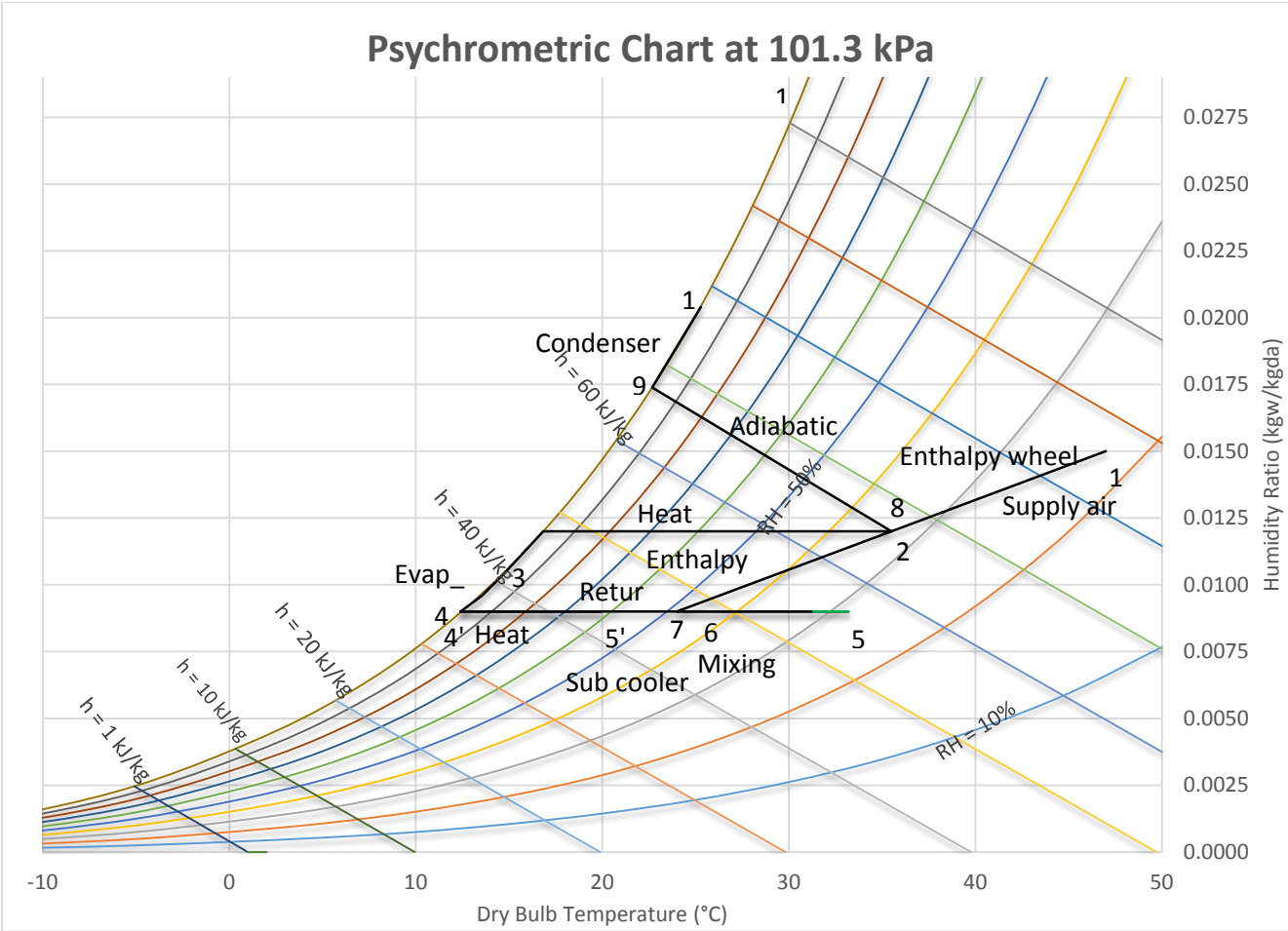

Figure 6: Third case: EW sensible effectiveness = 0.5, EW latent effectiveness = 0.5, HW effectiveness = 0.9, outdoor air at 47 °C, 15 g/kg

In the third case shown in Figure 6, heat wheel effectiveness is increased to .9 while keeping the enthalpy wheel sensible and latent effectiveness constant. In this case heat wheel removes the sensible load completely and a part of latent load. The evaporator load in this case is only a part of latent load. Therefore, for a given enthalpy wheel effectiveness, it can be observed that evaporator load is inversely proportional to heat wheel effectiveness.

However, a mechanism needs to be established to remove the water from the heat wheel for effective heat transfer and also to get enough water to make the necessary water balance to achieve closed DOAS.

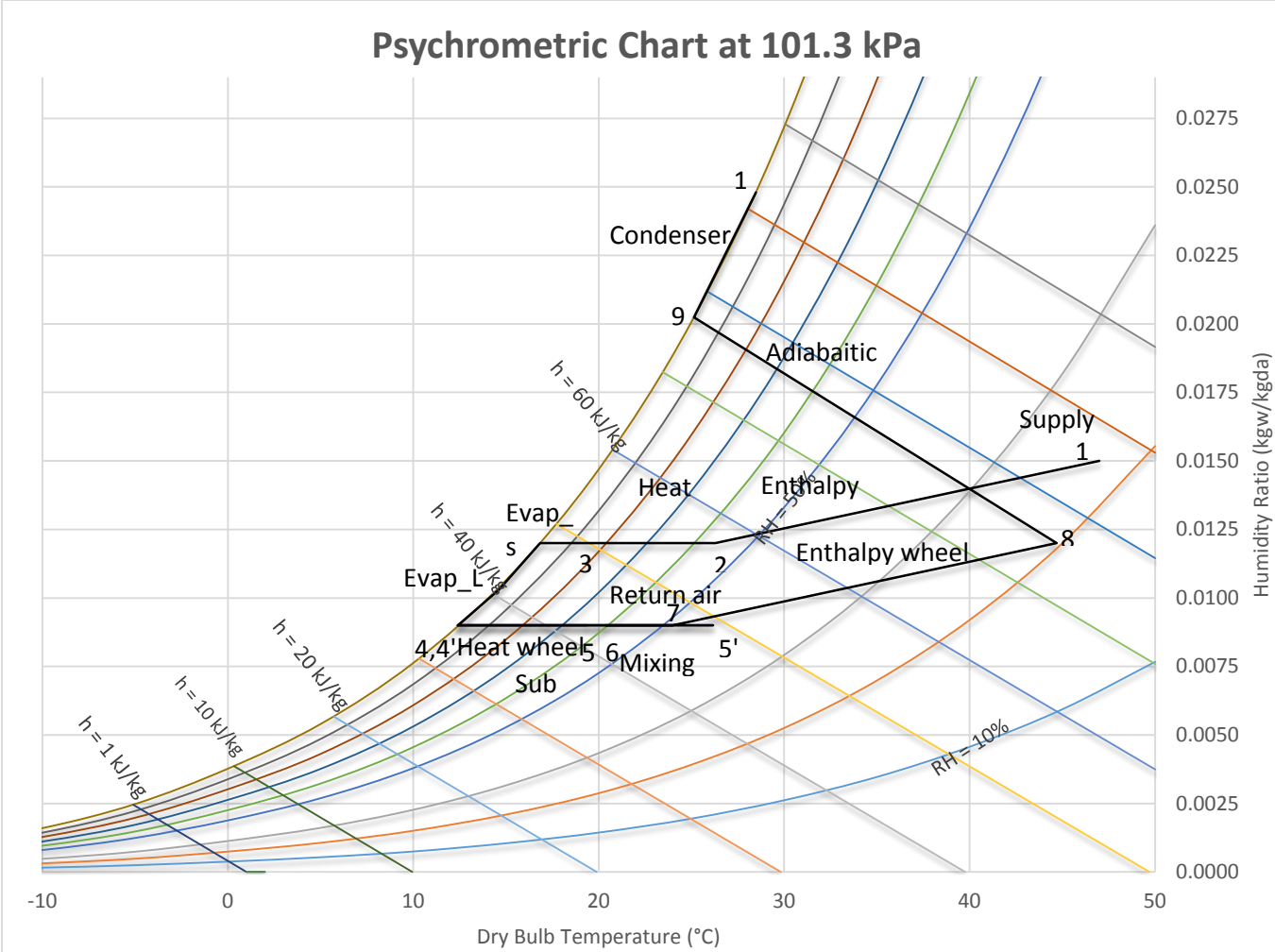

Figure 7: Fourth case: EW sensible effectiveness = 0.9, EW latent effectiveness = 0.5, HW effectiveness = 0.5, outdoor air at 47 °C, 15 g/kg

Keeping the heat wheel effectiveness and enthalpy wheel latent effectiveness constant while changing the enthalpy wheel sensible effectiveness as illustrated by Figure 4 and Figure 7, it can be observed that the sensible cooling required by the evaporator to bring the air close to its dew point temperature is decreased with an increase in the enthalpy wheel sensible effectiveness i.e. heat of evaporation is inversely related to enthalpy wheel sensible effectiveness.

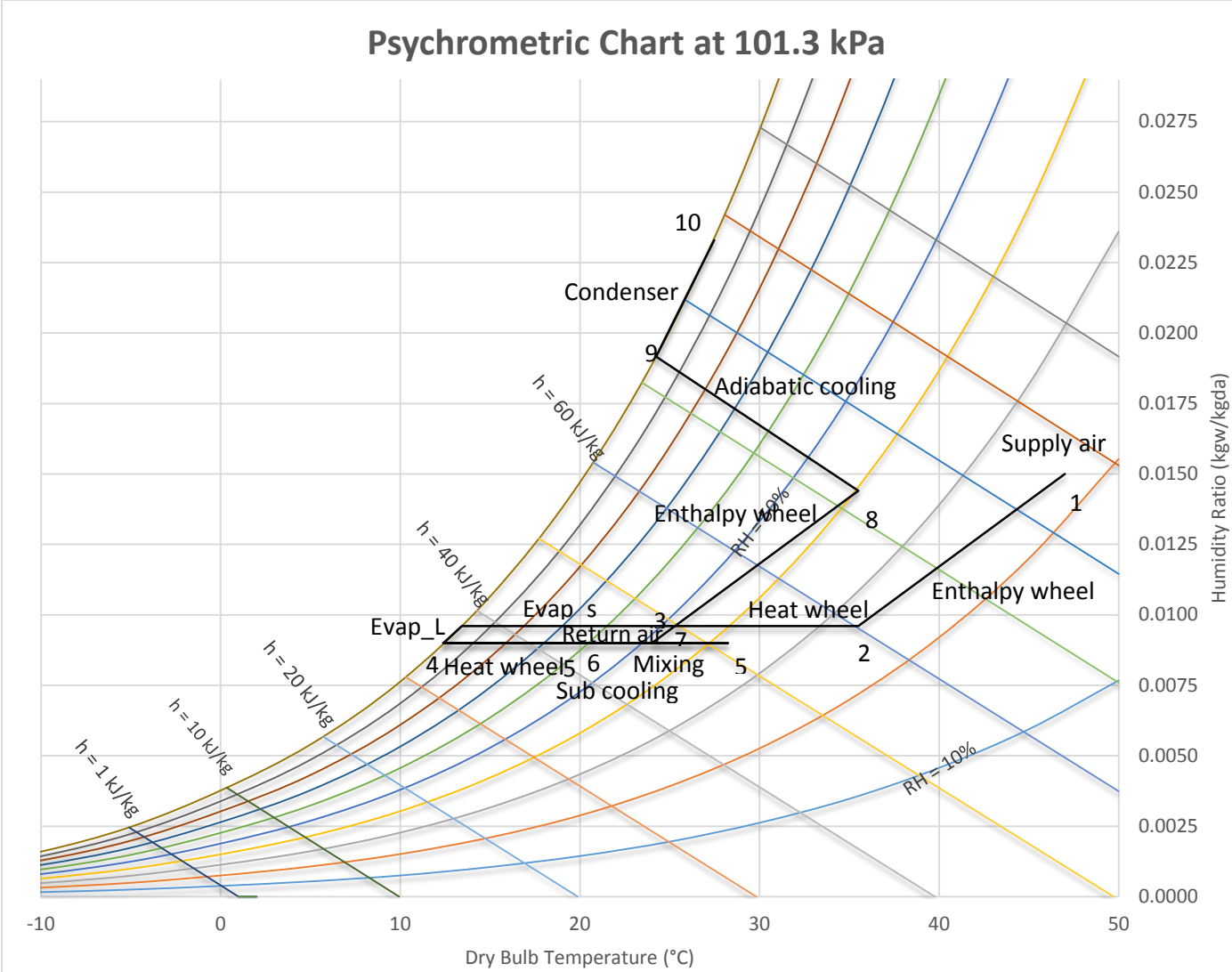

Figure 8: Fifth case: EW sensible effectiveness = 0.5, EW latent effectiveness = 0.9, HW effectiveness = 0.5, outdoor air at 47 °C, 15 g/kg

Keeping the heat wheel effectiveness and enthalpy wheel sensible effectiveness constant while changing the enthalpy wheel latent effectiveness as illustrated by Figure 4 and Figure 8, it can be observed that the latent cooling required by the evaporator is decreased with an increase in the enthalpy wheel sensible effectiveness due to the removal of moisture in the enthalpy wheel. However, the water balance required for closed DOAS is not possible in this configuration due to the removal of moisture mainly in the enthalpy wheel and very little moisture is condensed in the evaporator. Therefore, condensed water from the evaporator is not adequate enough for adiabatic cooling of air and keeping the condenser coils wet all the time.

Results for all Cases

For all cases return air enters the DOAS at T = 24C and w = 9g/kg. Four outdoor conditions are considered: w = 15 and 30 g/kg at T = 32 and w = 15 and 30 g/kg at T = 47C. Three values of design effectiveness are considered for each wheel: 0, 0.5 and 0.9, leading to 27 possible combinations of EW and HW effectiveness. The results for all cases are summarized in Table 1.

Table 1: Result for all cases

ε_{HW}	ε_{EW}		Outdoor air conditions		$\frac{\dot{m}_{req}}{\dot{m}_{avail}}$	Qevap	Air condition after Heat Wheel
	Sensible	Latent	Temp	Humidity		Kw	
0	0	0	32	30	2.9148652	11.42	un-sat
0	0	0	47	15	3.8585918	16.14	un-sat
0	0	0	47	30	1.8172715	28.9	un-sat
0	0.5	0	32	30	1.531394	22.38	Sat
0	0.5	0	32	15	2.8584725	10.08	un-sat
0	0.5	0	47	15	3.6699115	12.36	un-sat
0	0.5	0	47	30	1.7700434	24.95	un-sat
0	0.9	0	32	30	1.4905654	21.28	Sat
0	0.9	0	32	15	2.7773316	9.012	un-sat
0	0.9	0	47	30	3.4826093	21.79	Sat
0.5	0	0	32	30	1.3440606	20.38	Sat
0.5	0	0	32	15	2.2967246	8.142	un-sat
0.5	0	0	47	15	2.8092066	10.46	un-sat
0.5	0	0	47	30	1.5166327	22.96	Sat
0.5	0.5	0	32	30	1.3645971	19.7	Sat
0.5	0.5	0	32	15	2.3239912	7.437	Sat
0.5	0.5	0	47	15	2.9072348	8.566	un-sat
0.5	0.5	0	47	30	1.5353343	20.98	Sat
0.5	0.9	0	32	30	1.3662277	19.15	Sat
0.5	0.9	0	32	15	2.3501282	6.937	Sat
0.5	0.9	0	47	15	3.0171994	7.055	Sat
0.5	0.9	0	47	30	1.5717647	19.4	Sat
0.9	0	0	32	30	1.1967657	17.69	Sat
0.9	0	0	32	15	1.7403766	5.518	Sat
0.9	0	0	47	15	1.8484412	5.909	Sat
0.9	0	0	47	30	1.2240777	18.21	Sat
0.9	0.5	0	32	30	1.233884	17.55	Sat
0.9	0.5	0	32	15	1.8818985	5.384	Sat
0.9	0.5	0	47	15	2.2684508	5.531	Sat

0.9	0.5	0	47	30	1.3627736	17.81	Sat
0.9	0.9	0	32	30	1.264441	17.44	Sat
0.9	0.9	0	32	15	1.9991561	5.277	Sat
0.9	0.9	0	47	15	2.6342419	5.229	Sat
0.9	0.9	0	47	30	1.4737159	17.49	Sat
0	0	0.5	32	30	1.8524525	15.12	un-sat
0	0	0.5	32	15	4.5366072	8.957	un-sat
0	0	0.5	47	15	6.4924248	13.69	un-sat
0	0	0.5	47	30	2.4555803	20.18	un-sat
0	0.5	0.5	32	30	1.7377575	13.77	un-sat
0	0.5	0.5	32	15	4.3440014	7.625	un-sat
0	0.5	0.5	47	15	6.022573	9.935	un-sat
0	0.5	0.5	47	30	2.2789579	16.3	un-sat
0	0.9	0.5	32	30	1.6963946	12.69	un-sat
0	0.9	0.5	32	15	4.1947705	6.56	un-sat
0	0.9	0.5	47	15	5.7767772	6.928	un-sat
0	0.9	0.5	47	30	2.1939078	13.2	un-sat
0.5	0	0.5	32	30	1.4282334	11.81	Sat
0.5	0	0.5	32	15	3.183638	5.69	un-sat
0.5	0	0.5	47	15	4.2240045	8.04	un-sat
0.5	0	0.5	47	30	1.7602032	14.34	un-sat
0.5	0.5	0.5	32	30	1.4260249	11.14	Sat
0.5	0.5	0.5	32	15	3.2596737	5.028	un-sat
0.5	0.5	0.5	47	15	4.4780216	6.16	un-sat
0.5	0.5	0.5	47	30	1.8151895	12.4	Sat
0.5	0.9	0.5	32	30	1.450131	10.6	Sat
0.5	0.9	0.5	32	15	3.3283247	4.495	un-sat
0.5	0.9	0.5	47	15	4.7386302	4.65	un-sat
0.5	0.9	0.5	47	30	1.9154263	10.85	Sat
0.9	0	0.5	32	30	1.1370382	9.1696	Sat
0.9	0	0.5	32	15	2.0534574	3.0836	Sat
0.9	0	0.5	47	15	2.2731649	3.5167	Sat
0.9	0	0.5	47	30	1.1938515	9.6756	Sat
0.9	0.5	0.5	32	30	1.1736419	9.0347	Sat
0.9	0.5	0.5	32	15	2.3622096	2.9504	Sat
0.9	0.5	0.5	47	15	3.1830621	3.1409	Sat
0.9	0.5	0.5	47	30	1.442833	9.2877	Sat
0.9	0.9	0.5	32	30	1.2524561	8.9267	Sat
0.9	0.9	0.5	32	15	2.6164319	2.8438	Sat
0.9	0.9	0.5	47	15	3.9641305	2.8402	Sat
0.9	0.9	0.5	47	30	1.691696	8.9773	Sat

0	0	0.9	32	30	8.080414	8.9267	un-sat
0	0	0.9	32	15	25.102248	2.8438	un-sat
0	0	0.9	47	15	34.999743	2.8402	un-sat
0	0	0.9	47	30	11.061019	8.9773	un-sat
0	0.5	0.9	32	30	5.4546724	6.8877	un-sat
0	0.5	0.9	32	15	24.199033	5.6585	un-sat
0	0.5	0.9	47	15	32.807832	7.9944	un-sat
0	0.5	0.9	47	30	14.208423	9.3809	un-sat
0	0.9	0.9	32	30	11.336133	5.8239	un-sat
0	0.9	0.9	32	15	23.499972	4.5975	un-sat
0	0.9	0.9	47	15	31.217139	5.0005	un-sat
0	0.9	0.9	47	30	13.883314	6.3225	un-sat
0.5	0	0.9	32	30	6.0657824	4.9595	un-sat
0.5	0	0.9	32	15	18.253384	3.7355	un-sat
0.5	0	0.9	47	15	23.523103	6.1069	un-sat
0.5	0	0.9	47	30	7.622091	7.4528	un-sat
0.5	0.5	0.9	32	30	3.9159281	4.2947	un-sat
0.5	0.5	0.9	32	15	18.713365	3.0723	un-sat
0.5	0.5	0.9	47	15	25.002898	4.2358	un-sat
0.5	0.5	0.9	47	30	11.912742	5.5413	un-sat
0.5	0.9	0.9	32	30	10.121066	3.7628	un-sat
0.5	0.9	0.9	32	15	19.118498	2.5419	un-sat
0.5	0.9	0.9	47	15	26.462555	2.7388	un-sat
0.5	0.9	0.9	47	30	12.502231	4.0121	un-sat
0.9	0	0.9	32	30	4.5628747	2.3533	un-sat
0.9	0	0.9	32	15	12.530929	1.136	un-sat
0.9	0	0.9	47	15	13.643636	1.6031	un-sat
0.9	0	0.9	47	30	4.8552867	2.8519	un-sat
0.9	0.5	0.9	32	30	2.6803027	2.2203	Sat
0.9	0.5	0.9	32	15	14.172392	1.0034	un-sat
0.9	0.5	0.9	47	15	18.45917	1.2289	un-sat
0.9	0.5	0.9	47	30	10.07373	2.4696	un-sat
0.9	0.9	0.9	32	30	9.1485905	2.1139	Sat
0.9	0.9	0.9	32	15	15.518325	0.8973	un-sat
0.9	0.9	0.9	47	15	22.553818	0.9295	un-sat
0.9	0.9	0.9	47	30	11.395876	2.1638	Sat

Discussion

Based on the foregoing results we make the following observations:

- Changing heat wheel effectiveness while keeping enthalpy wheel(latent and sensible) effectiveness constant will not affect the amount of water we are getting in evaporator because w remains constant in heat wheel and evaporator leaving condition is fixed (24C and 9 g/kg). Heat wheel effectiveness will affect the Q_{evap} to the extent that it reduces sensible cooling load. By choosing a reasonable value of heat wheel design effectiveness (e.g. around 0.5), we can ensure that air leaving the HW is almost saturated and $Q_{evap}$is close to Q_{latent} .

- As a corollary to the previous point, note that of all cases with insufficient water supply, the shortages are generally least when the evaporator inlet condition is near or at saturation.

- Changing the enthalpy wheel latent effectiveness while keeping enthalpy wheel sensible and heat wheel effectiveness constant will affect the amount of water obtained in evaporator as well as amount of water required in condenser. For higher values of enthalpy wheel latent effectiveness, air entering the evaporator will have lower value of absolute humidity, leading to higher SHR, and air entering the condenser will have higher value of absolute humidity, so more water will generally be required for condensation than can be produced by evaporator.

- For the two outside air conditions where absolute humidity is high i.e. 30 g/kg, the amount of water produced by the evaporator is closer to water amount required for condensation as compared to air conditions where absolute humidity is low i.e. 15 g/kg.

- As EW and HW effectiveness increase, the evaporator load is greatly reduced. Thus, although the water balance leaves a shortage, the amount of additional water needed to evaporatively cool the condenser becomes quite small.

In response to the last point, we will relax the closed system constraint and evaluate the performance of a DOAS with evaporatively-cooled condenser in the return air stream that required a small external water supply.

3. Life Cycle Cost Optimized Design for GCC Weather

GCC Weather Data Description:

GCC cities TMY weather data is taken from the ASHRAE's IWEC2 files which represents the only collection of TMY weather data currently available for the GCC countries. A total of 48 IWEC2 files have been compiled by ASHRAE for the GCC countries. 24 TMY files were chosen based on the station's data quality ranking and geographical region covered. The data quality is based on the number of observed records for at least dry-bulb temperature, dewpoint temperature, cloud cover, and wind speed. Only weather stations with data quality A (greater than 7000 records) and B (greater than 3000 records) were used while stations with a data quality ranking of 'C' which represents reported measured data of less than 3000 records out of 8760 in a year were not considered. Table 2 gives the details of the chosen stations along with their weather design data:

Table 2: GCC Stations Information

Country	Station	Lat	Long	Elev (m)	StdP (kPa)	Evaporation WB/MCDB (°C)		24 Years Max WB (°C)	24 years Max DB (°C)		Cooling Degree Hours Base 18.3 °C	Moist Degree Hours Base 9g/kg
						WB	MCDB		Min	Max		
UAE	Abu Dhabi Intl. Airport	24.43	54.65	27	101.00	30.5	35.3	33.8	8.4	47.2	83126	41372
UAE	Al Ain Intl. Airport	24.27	55.60	265	98.18	29.1	36.2	32.5	8.6	47.5	92446	23531
BHR	Bahrain Intl. Airport	26.27	50.65	2	101.30	31.1	35.5	34.1	9.2	44.2	75052	47093
KWT	Kuwait Intl. Airport	29.22	47.98	48	100.75	28.5	35.1	32.2	1.4	49.8	83443	5265
OMN	Masirah	20.67	58.90	19	101.10	28.6	32.3	34.5	14.5	41.1	69674	59388
OMN	Seeb Intl Airport	23.58	58.28	15	101.14	30.4	33.9	34.0	12.8	46.2	70254	57308
OMN	Salalah	17.03	54.08	23	101.05	27.9	30.5	29.8	14.8	39.6	85906	50076
OMN	Thumrait	17.67	54.02	467	95.84	25.1	33.2	32.3	6.7	44.2	71190	22700
QAT	Doha Intl. Airport	25.25	51.57	10	101.20	31.1	35.2	33.9	9.3	47.0	82954	38513
SAU	Abha	18.23	42.65	2093	78.58	19.8	24.1	25.9	2.8	32.7	20285	13898
SAU	Makkah	21.43	39.77	240	98.47	28.9	38.6	32.2	13.2	47.9	47355	4280
SAU	Al-Madinah	24.55	39.70	636	93.91	22.1	36.6	27.3	6.1	46.5	57029	237
SAU	Tabuk	28.38	36.60	768	92.43	21.1	36.5	29.8	-0.7	42.7	92165	880
SAU	Al-Baha	20.30	41.65	1652	82.99	21.3	30.1	29.3	4.6	38.0	77199	1035
SAU	Al-Jouf	29.78	40.10	689	93.32	20.5	40.0	23.6	-2.9	44.8	60218	41886
SAU	Al-Qaisumah	28.32	46.13	358	97.10	22.8	39.7	29.6	0.1	48.3	59906	259
SAU	Al-Wejh	26.20	36.48	24	101.04	29.9	32.9	33.5	9.9	41.9	79073	23557

SAU	Dhahran	26.27	50.17	17	101.12	31.1	35.8	36.2	5.4	47.4	104762	85341
SAU	Gizan	16.88	42.58	7	101.24	30.5	36.3	34.5	18.2	40.6	85850	48499
SAU	Jeddah (King Abdul Aziz Intl. Airport)	21.70	39.18	17	101.12	29.9	35.0	35.0	13.2	45.5	76369	552
SAU	King Khaled Int. Airport	24.93	46.72	614	94.16	21.0	38.1	24.9	0.7	46.3	108620	33420
SAU	Sharorah	17.47	47.10	725	92.91	27.5	39.7	32.2	4.7	44.1	90856	3195
SAU	Arar	30.90	41.13	549	94.90	23.0	40.2	25.9	-2.3	45.1	51867	353
SAU	Yenbo	24.13	38.07	10	101.20	30.5	36.1	33.7	8.9	46.9	81325	36328

Ventilation Load Description:

A typical building of 227m^2 is considered having two zones with a total of 15 occupants. A ventilation rate of 5L/s/occupant with an area adjustment ventilation rate of 0.9L/s/m^2 is considered based on ASHRAE 62.1 (2010). The resulting zone ventilation rates of 18.3L/s/occupant and 19.26L/s/occupant were added to obtain the design flow rate of 0.265m^3/s at a maximum occupancy fraction of 95%.

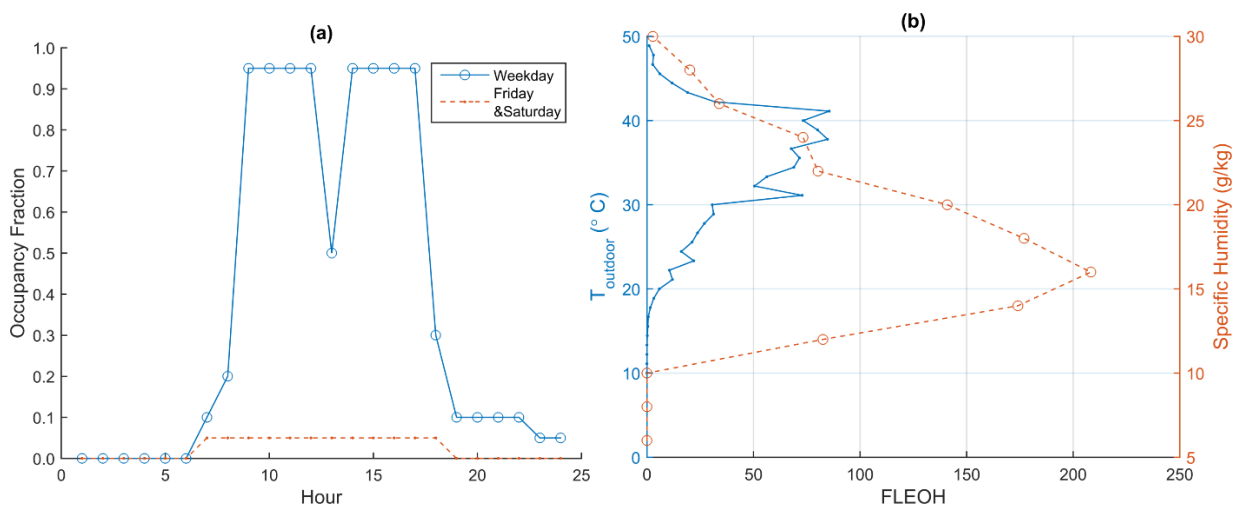

Figure 9: (a) Test building's occupancy schedule (b) Ventilation load FLEOH vs. Temperature and Specific Humidity

Figure 9 presents the occupancy schedule of a typical office building and the resulting ventilation load expressed in Full Load Equivalent Operating Hours (FLEOH). The cooling load is calculated based on setpoint supply specific humidity of 9g/kg which corresponds to 24°C dry bulb temperature and 50% relative humidity. Cooling load is computed only for the points for which outside specific humidity was greater 9g/kg and outside air temperature greater than dewpoint temperature at 9g/kg i.e. 12.5°C. FLEOH are computed by summing the simulated hourly cooling loads for each bin described by Equation (26):

$$FLEOH\ (i,j) = \frac{\sum_{n=1}^{8760} Q_{i,j}(n)}{Q_{max}} \quad (26)$$

where,

i = bin index for outdoor temperature grid T_i ; j = bin index for specific humidity grid w_j

$Q_{i,j}(n)$ = n^{th}-hour cooling load if $T \in T_i$ and $w \in w_j$; Q_{max} is the peak hourly cooling load of the year

LCC-Optimized DOAS Performance for Abu Dhabi Weather:

Heat exchangers effectiveness optimization by size scaling is performed for the DOAS cases by running an annual hourly simulation for the ventilation load of a typical office building. A logarithmic grid between 2 and 12 NTU comprising of eight values is considered for the ERW and HW for LCC optimization. The scaling factors of ERW and HW are calculated at the design UA of 1.536kW/K and 1.264kW/K respectively at the design air flow rate. Table 3 presents the effectiveness grid of ERW and HW computed at the design air flow rate using the rating conditions described in AHRI Standard 1061 (2013) which are $T_{DBoutdoor}$ = 35°C, $T_{WBoutdoor}$ = 26°C, $T_{DBreturn}$ = 23°C, $T_{WBreturn}$ = 17°C.

Table 3: effectiveness grid of ERW and HW for DOAS LCC optimization

ERW	0.650	0.684	0.742	0.791	0.833	0.867	0.895	0.918
HW	0.681	0.733	0.780	0.822	0.858	0.888	0.914	0.934

The ERW and HW cost function is given by Equations (27) and (28) based on OEM (DRI ROTOR) cost data. The DOAS life is considered to be 20years with a discount rate of 10%. An electricity cost of 8.9 cents/kWh is considered to calculate the yearly operating cost.

$$ERW\ cost\ (\$) = 677.87 + 407.78 * ERWscale \quad (27)$$

$$HW\ cost\ (\$) = 660.37 + 133.16 * HWscale\ (28)$$

Each DOAS is evaluated at the 64 points to compute the Net Present Value (NPV) given by Equation (29):

$$\mathrm{NPV}(\$) = \mathrm{DX\ electricity\ consumption(kWh)} * \mathrm{electricity\ cost(\$/kWh)} * \mathrm{Annuity\ factor} + \mathrm{ERW\ cost} + \mathrm{HW\ cost} \quad (29)$$

The Seasonal Efficiency Rating (SEER) rating is calculated by computing the cooling load across the DOAS based on the difference between outside air enthalpy and return air enthalpy and dividing by the sum of cooling and reheat electricity power consumption of the DOAS system. The return air enthalpy is calculated by adding the occupancy load to the supply setpoint temperature and specific humidity.

Table 4: Energy Performance Summary of LCC optimized Figure 1 DOAS cases

Annual Energy End Use	Cooling Energy (kWh)	DX Unit Energy (kWh)	Reheat Energy (kWh)	Total Energy (kWh)	SE	NPV ($)	Energy Savings/Year @0.089¢/kWh ($)
Case (a): DOAS with ERW	12538.54	2506.52	7894.51	10401.03	1.21	5344.64	
Case (b): DOAS with ERW and HW in SA and RA	12538.54	1140.54	1046.88	2187.42	5.73	3646.32	731.01
Case (c): DOAS with ERW, HW across evaporator and air subcooler/reheater in series to HW	12538.54	986.21	949.20	1935.41	6.48	3157.32	753.44
Case (d): DOAS with ERW, HW across evaporator and water subcooler	12538.54	1018.74	1367.41	2386.15	5.25	3200.63	713.32
Case (e): DOAS with ERW, HW across evaporator and air subcooler/reheater in parallel to HW	12538.54	1075.84	729.32	1805.15	6.95	3276.65	765.03

Table 4 present the energy and cost performance of the optimized LCC DOAS designs for Abu Dhabi climate. The reheat energy is calculated by the difference in supply air temperature at the outlet of the last DOAS component in the supply stream and the desired setpoint of 24°C. The Seasonal Efficiency (SE) is calculated by dividing annual cooling load across the DOAS by the sum of cooling and reheat electricity energy required by the DOAS system. The return air enthalpy entering the DOAS is calculated by adding the sensible and latent occupancy load to the supply setpoint temperature and specific humidity respectively. It can be seen that placing a run-around HX across the cooling coil results in better performance than placing the HX across the supply and return streams which is one of the high efficiency configurations sold by DOAS manufacturers. Furthermore, the SE of placing a reheat coil in parallel with the HW, case (e) is found to be around 7% more efficient than placing the reheat coil in series to the HW after the evaporator, case (c). However, the DX energy consumption of case (e) increases due to reduction in recovery rate across the run-around heat exchanger resulting from unbalanced flow.

LCC optimization was done for the air subcooler cases and the conventional DOAS with ERW and HW in SA and RA for the 24 weather stations presented in Table 2. Figure 10(a) presents the latent cooling load profile for these stations expressed in terms of FLEOH defined by Equation (13). It can be seen from Figure 10(b) that for stations with FLEOH's less than 300, the effect of using ERW is not pronounced for the air subcooler cases. ERW effectiveness is found to be between 0.8-0.85 for climates having greater than 500 FLEOH for the air subcooler/reheater cases. HW effectiveness is found to range between 0.74-0.82 for air subcooler cases for climates with >300 FLEOHs. The HW effectiveness tends to reduce for higher FLEOH climates which can be attributed to condensation control resulting in bypass of heat wheel. The ERW and HW effectiveness for the conventional high efficiency DOAS was found to be optimum around 0.86. Figure 10 (d) and (e) suggests that A DOAS system is desirable for climates with FLEOHs above 500 where the system first cost and NPV increase with FLEOHs is not very significant.

LCC-Optimized DOAS Air Sub-cooler Cases and Conventional ERW and HW Case:

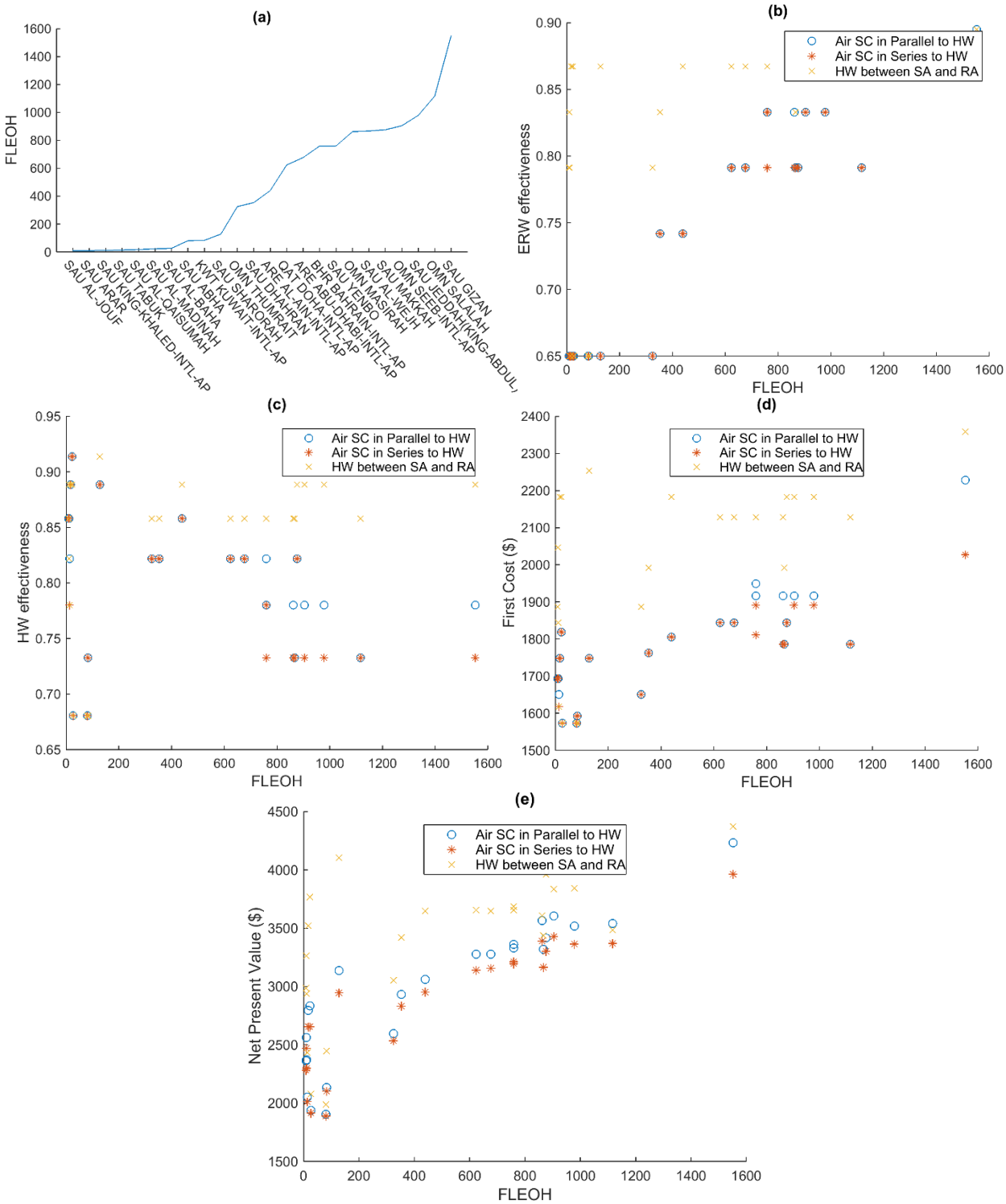

Figure 10: (a) GCC Weather Station FLEOHs. LCC optimized effectiveness for GCC weather stations: (b) ERW (c) HW, (d) LCC optimized first cost of ERW and HW and (e) LCC optimized NPV

4. Specification For Demonstration Unit

Experimental analysis needs to be performed for the air subcooler cases which represent the most energy savings compared to the conventional DOAS with only enthalpy wheel. A high-performance specification and corresponding design have been prepared in collaboration with a major supplier, DRI (DOAS manufacturer) for delivery of an experimental DOAS sized for handling the occupancy loads of MI Field Station test facility in Masdar City. Figure 11 shows the 3D sketch of the experimental DOAS system with components details presented in Table 5. Figure 11 (d) shows the top view of the experimental DOAS with the component numbers described in Table 5. The experimental DOAS is designed to test the air subcooler cases along with the closed DOAS case described in section 2.5. The experimental testing will enable us to validate the most efficient subcooler configuration and will serve as a test bed for providing data needed in training and refining the assumptions used in the current component models used for LCC optimization of DOAS.

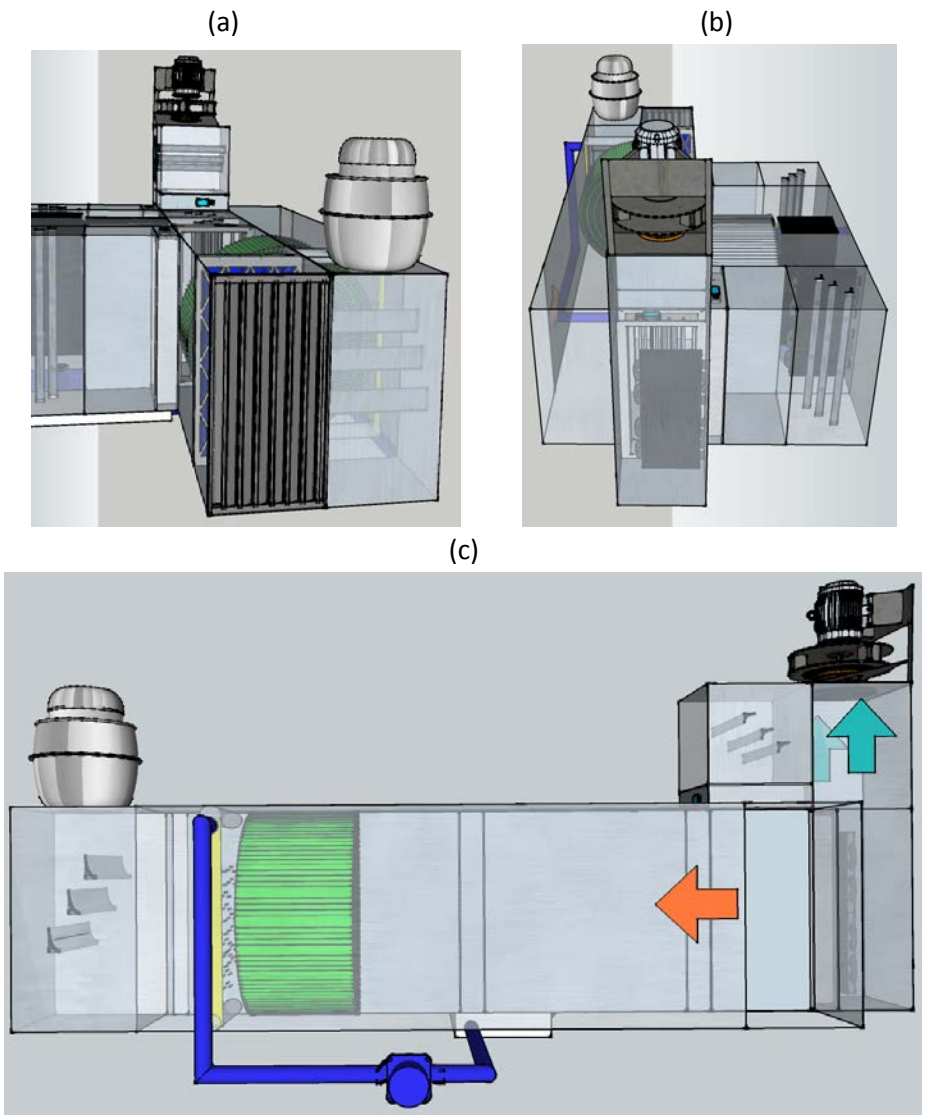

Figure 11: 3D views of experimental DOAS: (a) Front view (b) Back view (c) Side view

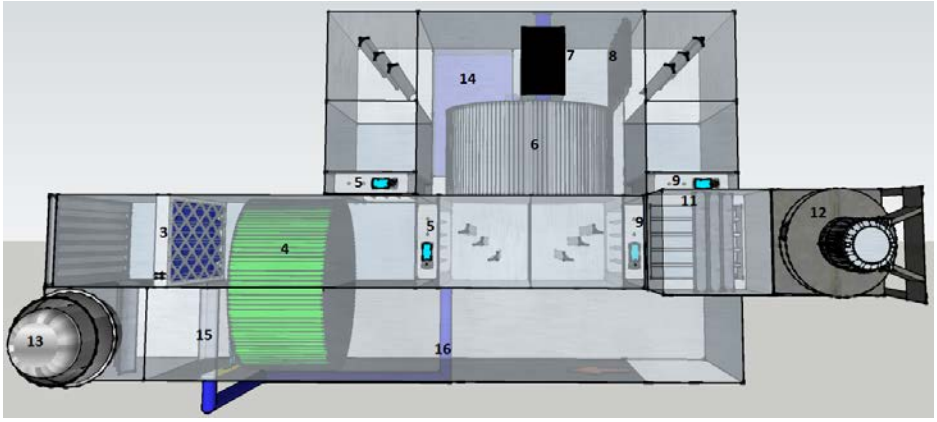

Figure 12: Top view of experimental DOAS view with component numbering according to Table 5

Table 5: DOAS components description

	Components	**Technical Description**
1	Duct Size	Equivalent to Enthalpy Wheel size
2	Evaporator Protrusion Size	Equivalent to Heat Wheel size
3	Air Filters	Depends on OEM. Can be on both supply and return
4	Enthalpy Wheel	0.85 effectiveness at 600cfm(0.265m3/s) and ARI conditions
5	Heat Wheel Face and Bypass Damper Hot Side	Tight shut-off rotary damper with linear control to 10% of air flow
6	Heat Wheel	0.82 effectiveness at 600cfm(0.265m3/s) and ARI conditions
7	DX Coil Evaporator	2 ton dehumidification capacity. Detailed design in Table 7
8	Subcooling Coil After Evaporator	0.1m2 tube inside area. Detailed design in Table 7
9	Heat Wheel Face and Bypass Damper Cold Side	Tight shut-off rotary damper with linear control to 10% of air flow
10	Subcooling Coil	0.1m2 tube inside area. Detailed design in Table 7
11	Subcooler Face and Bypass Damper	Tight shut-off rotary damper with linear control to 10% of air flow
12	Supply Plug Fan	600cfm(0.265m3/s) rated with variable speed down to 30cfm

13	Return Vertical Duct Fan	600cfm(0.265m3/s) rated with variable speed down to 30cfm
14	Water Collection Drain Pan	at least 15cm in height
15	Booster Pump With Float Switch And Atomizer System	20L/h maximum rating optimist system from Carel
16	Water Pipe To Supply Water To Return Side	1/4" PPR pipe
17	Electronic Expansion Valve	High efficiency inverter outdoor unit of 2 ton cooling capacity similar to mr. slim's MUY-GE24NA
18	Variable Speed Compressor Rated For 2ton Cooling Capacity	
19	Variable Speed Air Cooled Condenser	
20	Enthalpy Wheel VFD	Sized according to Enthalpy Wheel motor
21	Heat Wheel VFD	Sized according to Heat Wheel motor
22	Dampers Control	Linear control of Heat Wheel hot side and cold side based on THWout and condensation control. Subcooler damper control to maintain Tscout less than Tdesired. Split-ratio type control for face and bypass dampers
23	Temperature and Relative Humidity (RH) Sensors on Four Sides of Enthalpy Wheel	RH sensor accuracy +-5%, temperature sensors accuracy +-0.5C
24	Temperature Sensors on Four Sides of Heat Wheel	
25	Temperature Sensors on Two Sides of Subcooling Coil (Air Side)	
26	Speed Sensors For Enthalpy Wheel, Heat Wheel, Supply Fan And Return Fan	RPM accuracy +-1RPM
27	Electric Power Meters For Enthalpy Wheel, Heat Wheel, Fan, Compressor, Condenser Fan And Booster Pump	Power accuracy +-1%

Table 6: Preliminary detailed design of fin-tube heat exchangers used in the experimental DOAS

	tentative cooling coil specs	tentative subcooling coil specs
Height (m)	0.34	0.34
Width (m)	0.25	0.01
Depth (m)	0.68	0.68
Total Tubes	110	8
Tube Rows	4	1
Tube OD (m)	0.00635	0.00635
Tube Length (m)	0.68	0.68
Total Inside Area (m^2)	2.44	0.11
Horizontal Distance Between Tubes (m)	0.038	--
Vertical Distance Between Tubes (m)	0.02	0.04
Fins Per cm	8	10
Fin Thickness (mm)	0.1016	0.0762
Fin Type	straight	straight
Total Fin Area (m^2)	127.6	4.26

5. CONCLUSIONS

Different DOAS configurations to reduce the electrical energy consumption for satisfying the ventilation cooling demand are explored. In the second quarter progress report, it was found that elimination of reheat from the DOAS system with only ERW and an air-cooled chiller satisfying sensible cooling demand results in 15% annual total cooling energy savings for Abu Dhabi climate as compared to a conventional VAV system. Reheating coils for minimizing reheat energy have been proposed as early as (1966) by Rharnish. Different DOAS configurations for minimizing the reheating energy were explored which included using of an air-subcooler in parallel with HW, in series with HW, water-subcooler utilizing condensed water and using HW between supply and return air streams.

A methodology was also developed to generate performance maps of DX system independent of cooling load types encountered at the evaporator. The methodology was successfully applied to estimate annual energy performance of proposed DOAS configurations for the Abu Dhabi climate. It was found that placing the run-around HX across evaporator is more efficient than placing the HX between supply and return air streams. However, condensation control is required to avoid condensation in the run-around HX. It was also found that the energy efficiency of placing a reheat coil in parallel with the HW, case (e) is around 7% more efficient than placing the reheat coil in series to the HW after the evaporator, case (c). However, while reduced reheat energy results in 7% overall efficiency increase, the DX energy consumption of case (e) increases due to reduction in recovery rate across the run-around heat exchanger resulting from unbalanced flow.

An analysis of a closed DOAS system is done to check the feasibility of using condensed water to remove the heat of condensation from hot refrigerant in the condenser through evaporative cooling. Different combinations of ERW and HW effectiveness are explored to maximize the amount of condensed water without significant increase in cooling load and occurrence of condensation in the run-around rotary HX. It is found that for high absolute humidity conditions of around 30 g/kg, the amount of water produced by the evaporator is closer to the water amount required for condensation.

Lastly, LCC optimization is performed for finding optimum ERW and HW effectiveness and establishing a threshold for feasibility of using a separate DOAS system for latent load handling for GCC climates. The LCC optimization was done for the conventional high-efficient DOAS available in the market having ERW and HW between supply and return air stream, case (b), and for DOAS configurations with air-subcooler, case (c) and case (e). It was found that the optimum ERW and HW effectiveness for case (b) is around 0.86. For cases (c) and (e), ERW effectiveness is optimum around 0.8-0.85 for climates having greater than 500 FLEOH while HW effectiveness is found to range between 0.74-0.82. Installation of a separate ventilation system for handling latent load was found to be feasible for climates with greater than 500FLEOH where NPV curve vs. FLEOH become more flatter as compared to climates with lower FLEOH shown in Figure 10 (e).

A high performance DOAS specification for GCC climate was developed in collaboration with DRI ROTOR, a major global OEM for AHU with energy recovery wheels.

6. REFERENCES

AHRI Standard 1061: *Performance Rating of Air-to-Air Exchangers for Energy Recovery Ventilation Equipment*, Amer. Heating and Refrigeration Institute, 2013.

ANSI/ASHRAE 23–*Methods of Testing for Rating Positive Displacement Refrigerant Compressors and Condensing Units*, Amer. Soc. Heating, Refrigeration and Air-conditioning Engineers, 2005.

Ali, M.T., and P. R. Armstrong. 2015. Computationally Efficient Heat Pump Model to Accommodate Complex Load-Side Conditions or Configurations, *ASHRAE Annual Conference*, AT-15–C017. Atlanta, USA.

Ali, M.T., M.M. Mokhtar, M. Chiesa, P.R. Armstrong, (2011). A cooling change-point model of community-aggregate electrical load, *Energy and Buildings*, 43(1):28-37

Armstrong, P. R., W. Jiang, D. Winiarski, S. Katipamula, and L. K. Norford. 2009. "Efficient Low-Lift Cooling with Radiant Distribution, Thermal Storage, and Variable-Speed Chiller Controls—Part II: Annual Use and Energy Savings." *HVAC&R Research* 15 (2): 402–32.

ASHRAE. 2010. *62.1 User's Manual: ANSI/ASHRAE Standard 62.1-2010: Ventilation for Acceptable Indoor Air Quality*. ASHRAE.

Braun, J. E., S. A. Klein, and J. W. Mitchell. 1989. "Effectiveness Models for Cooling Towers and Cooling Coils." *ASHRAE Transactions* 95: 164–74.

Browne, M. W., and P. K. Bansal. 2001. "An Elemental ε-NTU Model for Vapour-Compression Liquid Chillers." *International Journal of Refrigeration* 24 (7): 612–27.

Cheung, H., and J. E. Braun. 2014. "Component-Based, Gray-Box Modeling of Ductless Multi-Split Heat Pump Systems." *International Journal of Refrigeration* 38: 30–45.

Coad, William J. 1999. "Conditioning Ventilation Air for Improved Performance and Air Quality." *Heating/piping/air Conditioning Engineering* 71 (9): 49–56.

Duggan, M. G., C. F. Hundy, and S. Lawson. 1988. "Refrigeration Compressor Performance Using Calorimeter and Flowrater Techniques." *International Compressor Engineering Conference*.

Eber, D. H., P. R. Glamm, D. L. Johnson, W. Earhart Jr, J. F. Klouda, B. J. Kiel, and D. A. Hulst. 2002. Refrigeration Circuit with Reheat Coil. 6,381,970, issued May 7, 2002. http://www.google.com/patents/US6381970.

Emmerich, S. J., and T. P. McDowell. 2005. "Initial Evaluation of Displacement Ventilation and Dedicated Outdoor Air Systems of US Commercial Buildings." NISTIR 7244. National Institute of Standards and Technology. http://fire.nist.gov/bfrlpubs/build05/PDF/b05011.pdf.

Fischer, John C., and Charlene W. Bayer. 2003. "Humidity Control in School Facilities." *Energy* 30: 35.

Friedrich, L.A. (2013). *An Urban Energy Baseline Model for Measurement & Verification of Building Energy Efficiency Retrofits in Abu-Dhabi*, MSESM Thesis, Masdar Institute of Science and Technology.

Gatley, D. P. 2000. "Dehumidification Enhancements." *Heating/Piping/Air Conditioning Engineering* 72 (9): 27–34.

Gayeski, N. T., P. R. Armstrong, and L. K. Norford. 2012. "Predictive Pre-Cooling of Thermo-Active Building Systems with Low-Lift Chillers." *HVAC&R Research* 18 (5): 858–73.

Hiller, C. C., and Leon R. Glicksman. 1976. “Improving Heat Pump Performance via Compressor Capacity Control: Analysis and Test.” MIT-EL, 76-001, MIT-EL, 76-002. MIT Energy Lab. http://dspace.mit.edu/handle/1721.1/27257.

Javed, H., O. Qureshi, M.T. Ali, and P.R. Armstrong. 2014. “Optimized Heat Pump Design for GCC Countries, Part I: Algorithm.” 11th IEA Heat Pump Conference, Montreal, Canada.

Jeong, Jae-Weon, and Stanley A. Mumma. 2003. “Impact of Mixed Convection on Ceiling Radiant Cooling Panel Capacity.” *HVAC&R Research* 9 (3): 251–57.

Jeong, J. W., S. A. Mumma, and W. P. Bahnfleth. 2003. “Energy Conservation Benefits of a Dedicated Outdoor Air System with Parallel Sensible Cooling by Ceiling Radiant Panels.” *ASHRAE Transactions* 109 (2): 627–36.

Katipamula, S. 1997. “A Review of Energy Savings Technology: Refrigerant Subcooling.” *Energy Engineering* 94 (3): 53–76.

Khattar, M., D. Shirey III, and R. Raustad. 2003. “Cool & Dry: Dual-Path Approach for a Florida School.” *ASHRAE Journal* 45 (5): 58–60.

Larrañaga, M. D., M. G. Beruvides, H. W. Holder, E. Karunasena, and D. C. Straus. 2008. “DOAS & Humidity Control.” *ASHRAE Journal* 50 (5): 34–41.

Lemmon, E. W., M. O. McLinden, and M. L. Huber. 2007. “REFPROP: Reference Fluid Thermodynamic and Transport Properties.” *NIST Standard Reference Database* 23 (8.0). http://thermosymposium.boulder.nist.gov/archive/symp17/pdf/Abstract_599.pdf.

Moore, T. 2008. “Potential and Limitations for Hydronic Radiant Slabs Using Waterside Free Cooling and Dedicated Outside Air Systems.” http://www.ibpsa.us/simbuild2008/technical_sessions/SB08-DOC-TS08-1-Moore.pdf.

Mumma, S. 2002. “Chilled Ceilings in Parallel with Dedicated Outdoor Air Systems: Addressing the Concerns of Condensation, Capacity, and Cost.” *ASHRAE Transactions* 108 (2): 220–31.

Mumma, S. A., and K. M. Shank. 2001. “Achieving Dry Outside Air in an Energy-Efficient Manner.” *ASHRAE Transactions* 107 (1): 553–61.

Mumma, Stanley A. 2001. “Overview of Integrating Dedicated Outdoor Air Systems with Parallel Terminal Systems.” http://citeseerx.ist.psu.edu/viewdoc/summary?doi=10.1.1.135.9149.

Mumma, Stanley A. 2010. “DOAS & Building Pressurization.” *ASHRAE Journal* 52 (8): 42.

Mumma, Stanley A., and J. Jeong. 2005a. “Field Experience Controlling a Dedicated Outdoor Air System.” *ASHARE Transactions* 111 (2): 433.

Mumma, S. A., and J. Jeong. 2005b. “Direct Digital Temperature, Humidity, and Condensate Control for a Dedicated Outdoor Air-Ceiling Radiant Cooling Panel System.” *ASHRAE Transactions* 111 (1): 547–58.

Mumma, S. A., and K. M. Shank. 2001. “Achieving Dry Outside Air in an Energy-Efficient Manner.” *ASHARE Transactions* 107 (1): 553–61.

Niu, J., J. V. D. Kooi, and H. Rhee. 1995. “Energy Saving Possibilities with Cooled-Ceiling Systems.” *Energy and Buildings* 23 (2): 147–58.

Rharnish, J. 1966. Air Conditioning Systems with Reheat Coils. 3,264,840, issued August 9, 1966. http://www.google.com/patents/US3264840.

Simonson, C. J., and R. W. Besant. 1999. “Energy Wheel Effectiveness: Part II—correlations” 42 (12): 2171–85.

Stetiu, Corina. 1999. “Energy and Peak Power Savings Potential of Radiant Cooling Systems in US Commercial Buildings.” *Energy and Buildings* 30 (2): 127–38.

Threlkeld, J. L. 1970. *Thermal Environmental Engineering*. Vol. 424. Prentice-Hall Englewood Cliffs, NJ. http://library.wur.nl/WebQuery/clc/282794.

Tian, Z. and J. A. Love. 2009. “Energy Performance Optimization of Radiant Slab Cooling Using Building Simulation and Field Measurements.” *Energy and Buildings* 41 (3): 320–30.

Trent, R. W. 2003. Advanced, Energy Efficient Air Conditioning, Dehumidification and Reheat Method and Apparatus. 6,658,874, issued December 9, 2003. http://www.google.com/patents/US6658874.

Wallin, J., H. Madani, and J. Claesson. 2012. “Run-Around Coil Ventilation Heat Recovery System: A Comparative Study between Different System Configurations.” *Applied Energy* 90 (1): 258–65.

Willingham, R. A. 2009. “Testing and Modeling of Compressors for Low-Lift Cooling Applications.” MS Thesis, Massachusetts Institute of Technology. http://web.mit.edu/parmstr/www/Theses/RAW-thesis-v7.pdf.

Wu, Z., R. V. N. Melnik, and F. Borup. 2006. “Model-Based Analysis and Simulation of Regenerative Heat Wheel.” *Energy and Buildings* 38 (5): 502–14.

Zakula, Tea, Nicholas Thomas Gayeski, Peter Ross Armstrong, and Leslie Keith Norford. 2011. “Variable-Speed Heat Pump Model for a Wide Range of Cooling Conditions and Loads” 17 (5): 670–91.

Zakula, T., N. T. Gayeski, P. R. Armstrong, and L. K. Norford. 2011. “Variable-Speed Heat Pump Model for a Wide Range of Cooling Conditions and Loads.” *HVAC&R Research* 17 (5): 670–91.

Zhang, L. Z. 2006. “Energy Performance of Independent Air Dehumidification Systems with Energy Recovery Measures.” *Energy* 31 (8): 1228–42.

Zhang, L. Z., D. S. Zhu, X. H. Deng, and B. Hua. 2005. “Thermodynamic Modeling of a Novel Air Dehumidification System.” *Energy and Buildings* 37 (3): 279–86.

Appendix A

Table A.1: Polynomial fit of R410a properties at saturated temperature for -5°C<x<50°C

	x^3	x^2	x	Intercept
Liquid Pressure (kPa)	0.00187	0.30170	25.55342	800.78858
Liquid Density (kg/m^3)	-0.00025	-0.01122	-4.01700	1169.92953
Gas Density (kg/m^3)	0.00026	0.00998	1.00415	30.62861
Liquid Specific Heat (kJ/kg.K)	0.00274	0.01319	5.45495	1520.25618
Liquid Viscosity (N.s/m^2)	0.00000	0.00000	0.00000	0.00016
Liquid Thermal Conductivity (W/m.K)	0.00000	0.00000	-0.00058	0.10309
Liquid Enthalpy (kJ/kg)	0.03362	2.04596	1522.04504	201219.58172
Gas Enthalpy (kJ/kg)	-0.05683	-2.70470	299.13024	422509.04373

Table A.2: 1/COP Polynomial Fit without fixed parts of compressor and condenser fan inverter loss

x1=CF; x2=Tx; x3=Te; Root Mean Squared Error: 4.39e-4

	Estimate	tStat	pValue		Estimate	tStat	pValue
Intercept	-6.219E-03	-6.008E-01	5.480E-01	**x1:x2^2**	-8.402E-05	-4.805E+00	1.613E-06
x1	7.872E-02	5.010E+00	5.694E-07	**x2^3**	1.996E-06	5.072E+00	4.139E-07
x2	7.438E-03	7.066E+00	1.901E-12	**x1^2:x3**	1.363E-03	1.312E+00	1.896E-01
x3	-5.063E-03	-4.823E+00	1.476E-06	**x1:x2:x3**	2.458E-04	3.711E+00	2.092E-04
x1^2	-8.056E-02	-4.779E+00	1.828E-06	**x2^2:x3**	4.944E-06	1.511E+00	1.308E-01
x1:x2	2.857E-03	3.300E+00	9.765E-04	**x1^4**	-5.498E-02	-8.451E+00	4.134E-17
x2^2	-6.822E-05	-1.902E+00	5.723E-02	**x1^3:x2**	1.249E-03	7.820E+00	6.888E-15
x1:x3	-4.476E-03	-3.371E+00	7.577E-04	**x1^2:x2^2**	4.282E-05	8.931E+00	6.564E-19
x2:x3	-2.235E-04	-2.326E+00	2.007E-02	**x1:x2^3**	1.788E-06	1.205E+01	8.166E-33
x3^2	1.078E-04	4.424E+00	9.965E-06	**x1^2:x2:x3**	-8.906E-05	-2.711E+00	6.746E-03
x1^3	1.174E-01	8.150E+00	4.952E-16	**x1:x2^2:x3**	-4.813E-06	-5.112E+00	3.357E-07
x1^2:x2	-2.670E-03	-5.131E+00	3.041E-07	**x2^3:x3**	-8.243E-08	-2.297E+00	2.169E-02

Table A.3: (Tcondliq-Tx)*CF^-0.6 Polynomial Fit for CF<=0.25

x1=CF; x2=Tx; x3=Te; Root Mean Squared Error: 0.0534. (Tcondliq rmse=0.0194K)

	Estimate	tStat	pValue		Estimate	tStat	pValue
(Intercept)	-2.450E+00	-3.255E-01	7.449E-01	**x1^2:x3**	2.585E+01	6.016E+00	2.289E-09
x1	-2.259E+02	-4.765E+00	2.085E-06	**x1:x2:x3**	-6.708E-02	-3.367E+00	7.815E-04
x2	-3.638E-01	-8.792E+00	4.326E-18	**x2^2:x3**	-1.676E-04	-3.075E+00	2.145E-03
x3	5.882E+00	2.759E+00	5.877E-03	**x1:x3^2**	3.227E+00	2.669E+00	7.705E-03
x1^2	3.887E+03	2.723E+01	6.942E-131	**x3^3**	1.687E-02	2.703E+00	6.959E-03
x1:x2	1.089E+01	1.696E+01	9.754E-59	**x1^4**	2.810E+04	2.802E+01	5.24E-137
x2^2	1.337E-03	2.003E+00	4.543E-02	**x1^3:x2**	4.926E+02	2.368E+01	2.96E-104
x1:x3	-3.736E+01	-2.903E+00	3.754E-03	**x1^2:x2^2**	2.327E-01	3.711E+00	2.145E-04
x2:x3	1.150E-02	3.481E+00	5.157E-04	**x1^3:x3**	-5.246E+01	-5.529E+00	3.848E-08
x3^2	-5.485E-01	-2.736E+00	6.309E-03	**x1:x2^2:x3**	1.064E-03	3.238E+00	1.234E-03

x1^3	-1.782E+04	-2.868E+01	3.861E-142	**x1:x3^3**	-9.985E-02	-2.653E+00	8.077E-03
x1^2:x2	-1.128E+02	-2.063E+01	1.363E-82	**x1^4:x2**	-7.228E+02	-2.279E+01	9.253E-98
x1:x2^2	-3.149E-02	-3.441E+00	5.975E-04	**x1^3:x2^2**	-7.268E-01	-5.250E+00	1.760E-07

43: (Tcondliq-Tx)*CF^-0.6 Polynomial Fit for CF>0.25

x1=CF; x2=Tx; x3=Te; Root Mean Squared Error: 0.0185. (Tcondliq rmse=0.0135K)

	Estimate	**tStat**	**pValue**		**Estimate**	**tStat**	**pValue**
(Intercept)	-4.036E+00	-6.802E-01	4.965E-01	**x1^2:x3**	3.551E+00	1.813E+00	6.992E-02
x1	2.583E+01	2.146E+00	3.202E-02	**x1:x2:x3**	-8.190E-03	-2.357E+00	1.850E-02
x2	-1.716E-01	-3.005E+00	2.685E-03	**x2^2:x3**	-4.313E-04	-2.738E+00	6.229E-03
x3	3.053E+00	1.852E+00	6.415E-02	**x1:x3^2**	4.093E-01	1.824E+00	6.831E-02
x1^2	-3.505E+01	-1.637E+00	1.018E-01	**x3^3**	8.845E-03	1.837E+00	6.637E-02
x1:x2	4.386E-01	2.852E+00	4.387E-03	**x1^4**	-1.629E+01	-1.875E+00	6.095E-02
x2^2	4.576E-03	2.595E+00	9.530E-03	**x1^3:x2**	2.285E-01	1.838E+00	6.613E-02
x1:x3	-5.602E+00	-2.233E+00	2.564E-02	**x1^2:x2^2**	7.509E-03	1.870E+00	6.162E-02
x2:x3	1.513E-02	3.290E+00	1.019E-03	**x1^3:x3**	-3.907E+00	-1.863E+00	6.256E-02
x3^2	-2.856E-01	-1.846E+00	6.497E-02	**x1^2:x2:x3**	6.177E-03	2.338E+00	1.946E-02
x1^3	4.137E+01	1.822E+00	6.866E-02	**x2^3:x3**	4.799E-06	2.753E+00	5.955E-03
x1^2:x2	-5.410E-01	-2.208E+00	2.738E-02	**x1:x3^3**	-1.268E-02	-1.815E+00	6.973E-02
x1:x2^2	-5.188E-03	-2.108E+00	3.515E-02	**x1^3:x2^2**	-3.666E-03	-1.789E+00	7.381E-02
x2^3	-5.017E-05	-2.665E+00	7.755E-03	**x1^4:x3**	1.448E+00	1.800E+00	7.204E-02